Journal of Sound and Vibration 469 (2020) 115139

Contents lists available at ScienceDirect

Journal of Sound and Vibration

journal homepage: www.elsevier.com/locate/jsvi

A two-stage Bayesian algorithm for finite element model updating by using ambient response data from multiple measurement setups

Çağlayan Hızal*, Gürsoy Turan

Department of Civil Engineering, Engineering Faculty of Izmir Institute of Technology, 35430, Urla, Izmir, Turkey

ARTICLE INFO

Article history:
Received 19 March 2019
Received in revised form 10 October 2019
Accepted 6 December 2019
Available online 9 December 2019
Handling Editor: K. Shin

Keywords:
Finite element model updating
Bayesian approach
Multiple setups
Operational modal analysis
Probability of damage

ABSTRACT

This study presents a two-stage Bayesian finite element model updating procedure by using acceleration response measurements obtained from multiple setups. In the presented methodology, parametric uncertainties for the modal parameters are estimated by using the Bayesian Fast Fourier Transform Approach (BFFTA). Different from the previous Bayesian methods, a block diagonal covariance matrix is modeled for prior estimation of measured modal parameters. In addition, the modelling error in the eigenvalue equations is considered as soft constraints to be updated. Numerical and experimental studies are presented to validate the proposed method. The effect of soft constraints on the identification results as well as their posterior uncertainties are investigated. According to the results, it is shown that the proposed methodology can identify the most probable finite element model parameters with high level of accuracy. In addition, the posterior uncertainties obtained by the proposed procedure are significantly small when compared to the methods that consider rigid constraints for prediction and/or modelling error.

1. Introduction

Finite element (FE) model updating has great importance in damage detection of structures and calibration of the considered mathematical models with respect to actual effects. While damage detection is possible with measured vibration response data only, FE model updating might be more effective on the detection of damage location and severity [1]. Various FE model updating approaches are available in the literature [2–8]. The most generic form of these approaches is based on the determination of system eigenvalues and eigenvectors that are best-fitted with measured (or identified) ones [1]. The problem of obtaining the best-fit between the measured and model parameters can be solved by single objective optimization based weighted least-squares. In the single objective optimization, the optimal weights can be correlated with parametric uncertainties. For this purpose, various stochastic model updating (SMU) methods have been employed by researchers within the past decades. SMU methods deal with the quantification of reducible and/or irreducible uncertainties based on statistical modelling. Here, reducible uncertainties are associated with the lack of information in mathematical model, environmental noise or insufficient experimental data. Irreducible uncertainties are induced by variability in material properties due to temperature, manufacturing effects, or possible changes in stiffness and/or mass parameters due to geometrical

* Corresponding author.
E-mail address: caglayanhizal@iyte.edu.tr (Ç. Hızal).

https://doi.org/10.1016/j.jsv.2019.115139
0022-460X/

configurations [9]. SMU approaches are generally based on maximum likelihood estimation of prediction error by using Monte Carlo Simulation (MCS) or Perturbation methods. MCS based methods define the reducible and irreducible uncertainties by using the statistical parameters from the multiple sets of experimental data. At the next step, a probability distribution is defined for modelling and measurement errors. MCS methods show high performance in the parameter estimation quality [10,11]. However, the computational cost is noted to be remarkably high which makes the implementation of MCS unreasonable especially for large mathematical models [12]. On the other hand, Perturbation methods considerably reduces computational effort when compared to MCS based approaches. However, the Perturbation methods have some limitations in terms of parameter estimation quality, since they consider small uncertainties for prediction error [9,13,14]. Various perturbation methods based on parameter-model variability estimation [15], or robust updating formulation by random matrix theory for uncertain computational models [16] are also available in the literature.

Bayesian probabilistic framework arises as another efficient and useful method for SMU [17–22]. In the conventional Bayesian FE model updating procedure, the optimal weights in the least-squares equation are associated with parameter error uncertainties obtained from measurements. This procedure requires updating the posterior most probable value by integrating the prior distributions over the whole parameter space [23]. This evaluation process was defined as difficult by Beck and Au [24] due to the large dimension for numerical integration, and a Markov Chain Monte Carlo Simulation (MCMCS) was employed to reduce the computational effort. In order to quantify the parametric uncertainties by multiple measurement sets under different environmental conditions, Hierarchical Bayesian methods have also been implemented in the literature [25]. In the Hierarchical Bayesian modelling, first a proper probability distribution is defined for the error equations between the identified and model-based parameters. Second, the posterior parameters of the constructed probability model are obtained by using direct integration, transitional [26] or evolutionary [27] MCMCS algorithm, Gibss sampling algorithm [28], or Metropolis Hasting method [29]. In addition, a two-stage Bayesian model updating procedure was proposed by Ching and Beck [30]. At the first step of the method, the modal identification procedure is completed, and experimental modal parameters are updated. At the next step, a prior distribution for stiffness parameters are defined, and finally most probable model parameters are obtained by applying Bayes' theorem [30]. This procedure is applied for both reference (undamaged) and damaged cases, and a damage extent is defined in order to measure the severity of damage level.

To reduce the computational effort in Bayesian FE model updating, Bayesian Operational Modal Analysis (BAYOMA) can also be employed for the estimation of parametric reducible uncertainties [31–33]. Estimation of the uncertainty of system parameters by BAYOMA eliminates the requirement of multiple sets of measurements and time-consuming methods such as MCS. Yuen and Kuok [34] presented a Bayesian FE model updating procedure based on the utilization of modal parameter data obtained by BAYOMA. A similar methodology was introduced by Yan and Katafygiotis [35] utilizing the multiple setup measurement data. In their study, only the local mode shape uncertainty obtained from BAYOMA is considered, and eigenvalues are assumed as well-estimated with zero uncertainty. When the uncertainty of eigenvalues is considered, the main problem in the Bayesian FE model updating incorporated with BAYOMA lies in the calculation of cross-correlation between the eigenvalues and eigenvectors. This problem is fundamentally induced by the scaling of eigenvectors. To overcome this problem some two-stage Bayesian algorithms have been presented to the literature [36–38]. These two-stage approaches consider an approximate block diagonal posterior covariance matrix for local modal parameters by using uncertainty laws for BAYOMA, and they are restricted to large values of signal-to-noise ratios, only. However, neglecting the off-diagonal elements may significantly change the values of the diagonal terms in the covariance matrix and it may lead to a rough estimation in the model updating procedure.

This study presents an alternative Bayesian FE model updating approach utilizing the ambient vibration data from multiple setup measurements. Consideration of mode shape norm constraints in the BAYOMA and Bayesian FE model updating procedure comes forward as the basic development upon the previous methods. The theory of the presented study is based on the modelling of the prior probability distribution for prediction error between the system (from FE model) and identified (from measurements) modal parameters by using BAYOMA. When compared to the previous Bayesian FE model updating methods that employ BAYOMA, the most important novelty of the presented study resides in the utilization of norm constraint equalities for local and global mode shape vectors (eigenvectors). By making use of this consideration, a zero correlation is derived between the eigenvalues and eigenvectors. Thus, the presented method works well not only for large signal-to-noise ratios but also for its lower values, and the computational effort is significantly reduced. The overall procedure rests on two stages. At first stage, the MPVs and posterior uncertainties of eigenvalues (frequencies) and eigenvectors (mode shapes) are derived by the Bayesian Fast Fourier Transform Approach (BFFTA). At second stage, system parameters (system modal and model parameters) including eigenvalues, eigenvectors, stiffness and mass scaling parameters are updated by using Bayesian inference. In addition, the modelling error in the eigenvalue equations and prior distributions for stiffness scaling parameters are considered. The resulting soft constraint approach, in which all uncertainty parameters are calculated within the procedure, is compared to the rigid constraint approximation (prescribed prediction and/or modelling error). According to the numerical study, the consideration of soft constraints results in significantly smaller posterior uncertainties. In addition, according to the laboratory experiments in which insufficient number of measurement points were used, the presented methodology gives reasonable results.

2. Stage I: modal identification

Eigenvalues and eigenvectors obtained from a FE model are expected to represent the whole structure. However, the modal information extracted from measurement data are constrained with the measurement points. In most cases, taking a full-scale measurement may not be possible due to the lack of instruments. The eigenvalues can be obtained with a reasonable accuracy by using a modal identification technique. However, the identified eigenvectors may not represent the system eigenvectors properly when insufficient measurement points are available only. This problem can be confronted by increasing the measurement setups. Thus, the posterior distribution of the modal parameters for each setup can be considered as a proper prior estimation for system eigenvalues and eigenvectors. For this purpose, first, BFFTA can be implemented to identify the most probable eigenvalues, eigenvectors, and their posterior uncertainties for the corresponding measurement setup. Second, their posterior probability distributions can be estimated by Gaussian approximation.

According to the fast BFFTA presented by Au [39], the negative logarithm-likelihood function for modal parameters to be identified, within the resonant frequency band of n^{th} mode, at the i^{th} setup, can be defined as follows,

$$L_{ni}(\boldsymbol{\Theta}_{ni}) = \; N_i N_{f,ni} \ln \pi + N_{f,ni}(N_i - 1)\ln S_{e,ni} + \sum_k \ln(\overline{S}_{ni} D_{k,ni} + S_{e,ni}) + S_{e,ni}^{-1}\kappa_{ni} - \boldsymbol{\phi}_{ni}^T \boldsymbol{\Delta}_{ni} \boldsymbol{\phi}_{ni}$$
$$\kappa_{ni} = \sum_k \mathbf{F}_{ki}^* \mathbf{F}_{ki}; \quad \boldsymbol{\Delta}_{ni} = \sum_k \frac{\overline{S}_i D_{k,ni} S_{e,ni}^{-1}}{(\overline{S}_{ni} D_{k,ni} + S_{e,ni})} \mathrm{Re}(\mathbf{F}_{ki} \mathbf{F}_{ki}^*) \tag{1}$$

where $L_{ni}(\boldsymbol{\Theta}_{ni})$ should be subjected to the constraint of $\boldsymbol{\phi}_{ni}^T \boldsymbol{\phi}_{ni} = 1$. In addition, $\boldsymbol{\Theta}_{ni} = [\lambda_{ni}, \xi_{ni}, \overline{S}_{ni}, S_{e,ni}, \boldsymbol{\phi}_{ni}]$, is the set of modal parameters to be identified and it comprises the eigenvalue (square of natural angular frequency), damping ratio, spectral density of modal excitation that is scaled with respect to the unit norm for local mode shape, spectral density of prediction error, and local mode shape vector (with unit norm), respectively. $\mathbf{F}_{ki}$ = Fast Fourier Transform (FFT) of acceleration response, N_i = number of measured degrees of freedom (DOF), $N_{f,ni}$ = number of data within the selected frequency band, and $D_{k,ni}$ denotes the dynamic amplification and it can be defined as follows,

$$D_{k,ni} = \left[(1 - \beta_{k,ni})^2 + 4\xi_{ni}^2 \beta_{k,ni} \right]^{-1}; \quad \beta_{k,ni} = \lambda_{ni} / \lambda_k; \quad \lambda_k = (2\pi f_k)^2 \tag{2}$$

where f_k = excitation frequency. Minimizing Eq. (1) gives the most probable modal parameters for the i^{th} setup. At the next step, the posterior probability distribution of the modal parameters can be well-estimated by using Gaussian approximation [39].

$$p(\boldsymbol{\Theta}_{ni} | \mathbf{Z}_{ki}) \approx \exp\left[-\frac{1}{2} (\boldsymbol{\Theta}_{ni} - \widehat{\boldsymbol{\Theta}}_{ni})^T \mathbf{H}_{\widehat{\Theta}_{ni}} (\boldsymbol{\Theta}_{ni} - \widehat{\boldsymbol{\Theta}}_{ni}) \right] \tag{3}$$

In Eq. (3), "$\widehat{\ }$" denotes the most probable value (MPV), $\mathbf{Z}_{ki} = [\mathrm{Re}(\mathbf{F}_{ki}); \mathrm{Im}(\mathbf{F}_{ki})] \in \Re$ is the augmented FFT vector of the measured response at the i^{th} setup, and $\mathbf{H}_{\widehat{\Theta}_{ni}}$ = Hessian of $L_{ni}(\boldsymbol{\Theta}_{ni})$ under the norm constraint for the mode shape vector, at $\boldsymbol{\Theta}_{ni} = \widehat{\boldsymbol{\Theta}}_{ni}$. Here, a zero correlation can be obtained between the spectrum parameters, $\boldsymbol{\Theta}_{s,ni} = [\lambda_{ni}, \xi_{ni}, \overline{S}_{ni}, S_{e,ni}]$ and $\boldsymbol{\phi}_{ni}$ due to the norm constraint equation. Using the computational scheme proposed by Au and Xie [40], $\mathbf{H}_{\widehat{\Theta}_{ni}}$ is derived as a block diagonal matrix after mathematical manipulations (see Appendix A).

$$\mathbf{H}_{\widehat{\Theta}_{ni}} = \begin{bmatrix} \mathbf{H}_{\widehat{\Theta}_{s,ni}} & 0 \\ 0 & \mathbf{H}_{\widehat{\phi}_{ni}} \end{bmatrix} \tag{4}$$

Here, $\mathbf{H}_{\widehat{\Theta}_{s,ni}} = \nabla^2 L^{(\widehat{\Theta}_{s,ni}, \widehat{\Theta}_{si})}$, and $\mathbf{H}_{\widehat{\phi}_{ni}} = \nabla^2 L^{(\widehat{\phi}_{ni}, \widehat{\phi}_{ni})} + 2\overline{\alpha}_{ni} \mathbf{I}_{Ni}$, ($\overline{\alpha}_{ni}$ = Lagrange multiplier that enforces the unit norm of $\widehat{\phi}_{ni}$). Note that Note that $\overline{\alpha}_{ni}$ corresponds to the maximum eigenvalue of $\nabla^2 L^{(\widehat{\phi}_{ni}, \widehat{\phi}_{ni})}$, and $\mathbf{H}_{\widehat{\phi}_{ni}}$ is a semi positive definite matrix whose eigenvector for the zero eigenvalue corresponds to $\widehat{\phi}_{ni}$ [41].

$$\overline{\alpha}_{ni} = -2\widehat{\boldsymbol{\phi}}_{ni}^T \nabla^2 L^{(\widehat{\phi}_{ni}, \widehat{\phi}_{ni})} \widehat{\boldsymbol{\phi}}_{ni} \quad ; \quad \widehat{\boldsymbol{\phi}}_{ni}^T \mathbf{H}_{\widehat{\phi}_{ni}} \widehat{\boldsymbol{\phi}}_{ni} = 0 \tag{5}$$

3. Stage II: model updating

At this stage, first, the prior probability distributions required for FE model updating are defined. Here, the prior probability distribution of eigenvalues and eigenvectors are modeled by the posterior probability estimation obtained from the modal identification stage. In addition, a prior probability distribution for modelling error in the eigenvalue equations is

considered in order to avoid the mode matching problem. Then, the probability distribution function (PDF) of the model parameters is estimated by using Bayes' theorem. Finally, the FE model is updated by maximum likelihood estimation of the posterior PDF that is obtained by Bayesian inference.

3.1. Prior probability distributions for eigenvalues and eigenvectors

In this study, the modal parameters (eigenvalues and eigenvectors) that are identified from the measurements are associated with those from the FE model. For this purpose, a set of system modal parameters that are obtained from the FE model can be defined by

$$\boldsymbol{\chi}_{ni} = \widehat{\boldsymbol{\chi}}_{ni} + \boldsymbol{\varepsilon}_{\chi ni} \tag{6}$$

where, $\boldsymbol{\chi}_{ni} = [\lambda_n, \ \ r_{ni}^{-1}\ \boldsymbol{\Gamma}_{oi}\boldsymbol{\Phi}_n]^T$, $\boldsymbol{\Gamma}_{oi}$ = selection matrix that extracts the measured DOFs at i^{th} setup, $\widehat{\boldsymbol{\chi}}_{ni} = [\widehat{\lambda}_{ni}, \ \widehat{\boldsymbol{\phi}}_{ni}]^T$ is the set of most probable local modal parameters obtained at the modal identification stage, and $\boldsymbol{\varepsilon}_{\chi ni}$ = prediction error. In addition, λ_n and $\boldsymbol{\Phi}_n$ denote the n^{th} mode eigenvalue and eigenvector (global mode shape vector) of the finite element model, respectively. The error term, $\boldsymbol{\varepsilon}_{\chi ni}$ can be assumed to follow a zero mean Gaussian distribution. Therefore, this distribution can be modeled by the posterior PDF of $\widehat{\boldsymbol{\chi}}_{ni}$. When $\boldsymbol{\varepsilon}_{\chi ni}$ is assumed to be linearly independent for each setup, the prior probability distribution of the prediction error can be written as

$$p\left(\boldsymbol{\varepsilon}_{\chi}|\widehat{\boldsymbol{\Theta}}_s\right) = \prod_{n=1}^{N_m}\prod_{i=1}^{N_s} p\left(\boldsymbol{\varepsilon}_{\chi ni}|\widehat{\boldsymbol{\Theta}}_{sni}\right) \approx \prod_{n=1}^{N_m}\prod_{i=1}^{N_s} exp\left\{ -\frac{1}{2}\left(\boldsymbol{\chi}_n - \widehat{\boldsymbol{\chi}}_{ni}\right)^T \mathbf{H}_{\widehat{\boldsymbol{\chi}}_{ni}} \left(\boldsymbol{\chi}_n - \widehat{\boldsymbol{\chi}}_{ni}\right) \right\} \tag{7}$$

where N_s = number of measurement setups, N_m = number of considered modes, $\widehat{\boldsymbol{\varepsilon}}_{\chi} = [\widehat{\boldsymbol{\varepsilon}}_{\chi 11}, \ldots, \widehat{\boldsymbol{\varepsilon}}_{\chi N_m N_s}]$, and $\widehat{\boldsymbol{\Theta}}_s = [\widehat{\boldsymbol{\Theta}}_{s11}, \ldots, \widehat{\boldsymbol{\Theta}}_{sN_mN_s}]$. In addition, $\mathbf{H}_{\widehat{\boldsymbol{\chi}}_{ni}}$ denotes the Hessian with respect to $\boldsymbol{\chi}_{ni}$ at $\boldsymbol{\chi}_{ni} = \widehat{\boldsymbol{\chi}}_{ni}$ and it can be estimated by the BFFTA. Thus, $\mathbf{H}_{\widehat{\boldsymbol{\chi}}_{ni}}$ can be written as a block diagonal matrix.

$$\mathbf{H}_{\widehat{\boldsymbol{\chi}}_{ni}} = \begin{bmatrix} H_{\widehat{\lambda}_{ni}} & \mathbf{0}_{1\times N_i} \\ \mathbf{0}_{N_i\times 1} & \mathbf{H}_{\widehat{\phi}_{ni}} \end{bmatrix} \tag{8}$$

3.2. Estimation of prior stiffness and mass distributions

To construct a more reasonable probabilistic model, the prior probability distribution of mass and stiffness scaling parameters of FE model can be selected as truncated Gaussian PDF because negative model parameter values are not expected.

The prior probability distributions for mass parameters are assumed to be linearly independent (zero correlation between each mass parameter). Thus, the prior PDF of mass scaling can be defined as below.

$$p(\boldsymbol{\rho}) = \prod_{r=1}^{N_\rho} p(\rho_r) \tag{9}$$

In Eq. (9), $\boldsymbol{\rho} = [\rho_1, \rho_2, \ldots \rho_{N\rho}]$ indicates the set of mass scaling parameters to be updated, $\rho_r = r^{th}$ mass scaling parameter, and N_ρ = number of mass parameters. Here, $p(\rho_r)$ can be defined as,

$$p(\rho_r) \propto \begin{cases} \exp\left\{ -\dfrac{(\rho_r - \widehat{\rho}_{r0})^2}{2S_{\widehat{\rho}_o}} \right\}, & \text{for} \quad \rho_r > 0 \\ 0\,, & \text{for} \quad \rho_r \le 0 \end{cases} \tag{10}$$

where $\widehat{\rho}_{r0}$ = prior MPV of r^{th} mass parameter, $S_{\widehat{\rho}_o}$ = constant prior variance for each mass parameter. Similarly, the prior probability distribution for stiffness parameters can be defined as below.

$$p(\boldsymbol{\theta}) = \prod_{r=1}^{N_\theta} p(\theta_r)$$

$$p(\theta_r) \propto \begin{cases} \exp\left\{ -\dfrac{(\theta_r - \widehat{\theta}_{r0})^2}{2S_{\widehat{\theta}_o}} \right\}, & \text{for} \quad \theta_r > 0 \\ 0\,, & \text{for} \quad \theta_r \le 0 \end{cases} \tag{11}$$

In Eq. (11), $\boldsymbol{\theta} = [\,\theta_1, \theta_2, \ldots\, \theta_{N\rho}]$ denotes the set of stiffness scaling parameters, $\theta_r = r^{th}$ stiffness scaling parameter, $\widehat{\theta}_{r0} =$ prior MPV of r^{th} stiffness scaling parameter, $S_{\widehat{\theta}_o}$ = constant prior variance for each stiffness scaling parameter, and N_θ = number of stiffness scaling parameters.

3.3. Prior probability distribution for modelling error

Considering a general eigenvalue-eigenvector problem for a particular mode, n, the following equality can be constructed for a modal updating problem,

$$\mathbf{K}(\boldsymbol{\theta})\boldsymbol{\Phi}_n = \lambda_n \mathbf{M}(\boldsymbol{\rho})\boldsymbol{\Phi}_n + \boldsymbol{\varepsilon}_m \tag{12}$$

in which $\mathbf{K}(\boldsymbol{\theta})$, $\mathbf{M}(\boldsymbol{\rho})$ are parametric stiffness and mass matrices, and ε_m = modelling error which is assumed to be identical for all modes. Assuming that ε_m follows a zero mean Gaussian distribution, the following PDF can be defined for a given set of system modal parameters, $\boldsymbol{\chi} = [\,\boldsymbol{\chi}_1, \ldots, \boldsymbol{\chi}_{N_m}]$,

$$p(\boldsymbol{\varepsilon}_m|\boldsymbol{\chi}) = (2\pi S_{\widehat{\varepsilon}})^{-N/2} \exp\left(\boldsymbol{\varepsilon}_m^T S_{\widehat{\varepsilon}}^{-1} \boldsymbol{\varepsilon}_m\right) \tag{13}$$

where $S_{\widehat{\varepsilon}}$ = expected variance of the modelling error which is assumed to be identical for each mode, and N = number of DOF in the finite element model. The modelling error can be defined in terms of mass and stiffness scaling parameters as

$$\boldsymbol{\varepsilon}_m = [\mathbf{K}(\boldsymbol{\theta}) - \lambda_n \mathbf{M}(\boldsymbol{\rho})]\boldsymbol{\Phi}_n = \boldsymbol{\Omega}_n \boldsymbol{\Phi}_n \tag{14}$$

in which the parametric stiffness and mass matrices are defined as

$$\mathbf{K}(\boldsymbol{\theta}) = \mathbf{K}_0 + \sum_{r=1}^{N_\theta} \theta_r \mathbf{K}_r \qquad \mathbf{M}(\boldsymbol{\rho}) = \mathbf{M}_0 + \sum_{r=1}^{N_\rho} \rho_r \mathbf{M}_r \tag{15}$$

where, K_0 and M_0 are N × N sized non-parametric components of stiffness and mass matrices, K_r, and M_r are N × N sized r^{th} non-parametric sub-structural stiffness and mass matrices, respectively. Substituting Eq. (14) into Eq. (13) leads to the following conditional PDF.

$$p(\varepsilon_m|\boldsymbol{\chi}) = \prod_{n=1}^{N_m} (2\pi S_{\widehat{\varepsilon}})^{-N/2} \exp\left(-\frac{1}{2} \boldsymbol{\Phi}_n^T \boldsymbol{\Omega}_n^T S_{\widehat{\varepsilon}}^{-1} \boldsymbol{\Omega}_n \boldsymbol{\Phi}_n \right) \tag{16}$$

3.4. Posterior probability distribution for system parameters

In this study, the model parameters (stiffness and mass scaling parameters) and system modal parameters are associated with the prediction and modelling error terms. Applying the Bayes' theorem, a posterior probability distribution for the model and system modal parameters can be defined as

$$p(\boldsymbol{\theta}, \boldsymbol{\rho}, \boldsymbol{\chi}|\varepsilon_\chi, \varepsilon_m) = c_0 \times p(\varepsilon_\chi|\boldsymbol{\chi}) \times p(\varepsilon_m|\widehat{\boldsymbol{\Theta}}_s) \times p(\boldsymbol{\theta}) \times p(\boldsymbol{\rho}) \tag{17}$$

where c_0 is a normalizing constant. Substituting Eqs. (7), (10), (11) and (16) into Eq. (17) and using the negative-logarithm likelihood function for the result, the maximum likelihood estimation is transformed into a minimization problem.

$$L(\boldsymbol{\theta},\boldsymbol{\rho},\boldsymbol{\chi}) = \frac{1}{2}\sum_{n=1}^{N_m}\sum_{i=1}^{N_s}\left(r_{ni}^{-1}\boldsymbol{\Gamma}_{oi}\boldsymbol{\Phi}_n - \widehat{\boldsymbol{\phi}}_{ni}\right)^T H_{\widehat{\phi}_i}\left(r_{ni}^{-1}\boldsymbol{\Gamma}_{oi}\boldsymbol{\Phi}_n - \widehat{\boldsymbol{\phi}}_{ni}\right) + \frac{1}{2}\sum_{n=1}^{N_m}\sum_{i=1}^{N_s}\left(\lambda_n - \widehat{\lambda}_{ni}\right)^2 H_{\widehat{\lambda}_{ni}}$$
$$+\frac{1}{2}\left(\boldsymbol{\theta} - \widehat{\boldsymbol{\theta}}_0\right)^T S_{\widehat{\theta}_o}^{-1}\left(\boldsymbol{\theta} - \widehat{\boldsymbol{\theta}}_0\right) + \frac{1}{2}\left(\boldsymbol{\rho} - \widehat{\boldsymbol{\rho}}_0\right)^T S_{\widehat{\rho}_o}^{-1}\left(\boldsymbol{\rho} - \widehat{\boldsymbol{\rho}}_0\right) \tag{18}$$
$$+\frac{1}{2}N_m N \ln 2\pi + \frac{1}{2}N_m N \ln S_{\widehat{\varepsilon}} + \frac{1}{2}\sum_{n=1}^{N_m}\boldsymbol{\Phi}_n^T\boldsymbol{\Omega}_n^T S_{\widehat{\varepsilon}}^{-1}\boldsymbol{\Omega}_n\boldsymbol{\Phi}_n$$

In Eq. (18), norm constraints should be defined for $\boldsymbol{\Gamma}_{oi}\boldsymbol{\Phi}_n$ and $\boldsymbol{\Phi}_n$. Thus, Eq. (18) leads to a linear optimization problem as below.

$$J(\boldsymbol{\theta},\boldsymbol{\rho},\boldsymbol{\chi},\boldsymbol{\alpha},\boldsymbol{\beta}) = L(\boldsymbol{\theta},\boldsymbol{\rho},\boldsymbol{\chi}) + \sum_{i=1}^{N_m}\sum_{i=1}^{N_s}\alpha_{ni}\left(\boldsymbol{\Phi}_n^T\boldsymbol{\Gamma}_{oi}^T\boldsymbol{\Gamma}_{oi}\boldsymbol{\Phi}_n - r_{ni}^2\right) + \beta_n\left(\boldsymbol{\Phi}_n^T\boldsymbol{\Phi}_n - 1\right) \tag{19}$$

where $\boldsymbol{\alpha} = [\boldsymbol{\alpha}_{11}, \ \ldots \ , \ \alpha_{N_m N_s}]$, and $\boldsymbol{\beta} = [\beta_1, \ \ldots \ , \ \beta_{N_m}]$ are sets of Lagrange multipliers for the norm constraints. MPV of system modal and model parameters can be estimated by minimizing Eq. (19).

3.4.1. MPV of system modal parameters

The posterior MPV of $\boldsymbol{\chi}$ is incorporated with measured response data as well as structural model parameters. Thus, the minimization process performs a posterior modal identification and model updating together. In this context, minimizing Eq. (19) with respect to λ_n, and $\boldsymbol{\Phi}_n$ gives the most probable system modal parameters incorporated with structural model parameters and measurements.

The first order derivative of Eq. (19) with respect to λ_n results in the following equation,

$$\left.\frac{\partial J}{\partial\lambda_n}\right|_{\lambda_n=\widehat{\lambda}_n} = 0 \quad \Rightarrow \quad \widehat{\lambda}_n = \left(S_{\widehat{\varepsilon}}^{-1}G_{\lambda_n} + \sum_{i=1}^{N_s}H_{\widehat{\lambda}_{ni}}\right)^{-1} \times \left(S_{\widehat{\varepsilon}}^{-1}g_{\lambda_n} + \sum_{i=1}^{N_s}H_{\widehat{\lambda}_{ni}}\widehat{\lambda}_{ni}\right) \tag{20}$$

where $\widehat{\lambda}_n$ = most probable eigenvalue for nth mode, $G_{\lambda_n} = \boldsymbol{\Phi}_n^T\mathbf{M}^T\mathbf{M}\boldsymbol{\Phi}_n$, and $g_{\lambda n} = \boldsymbol{\Phi}_n^T\mathbf{K}^T\mathbf{M}\boldsymbol{\Phi}_n$. Here, it is seen that $\widehat{\lambda}_n$ depends on $S_{\widehat{\varepsilon}}$, G_{λ_n} and $g_{\lambda n}$ which are initially unknown. For this reason, a proper initial guess for $\widehat{\lambda}_n$ is required. If the modelling error is neglected, an initial guess for λ_n can be obtained as follows.

$$\widehat{\lambda}_n = \left(\sum_{i=1}^{N_s}H_{\widehat{\lambda}_{ni}}\right)^{-1} \times \sum_{i=1}^{N_s}H_{\widehat{\lambda}_{ni}}\widehat{\lambda}_{ni} \tag{21}$$

Similarly, minimizing Eq. (19) with respect to $\boldsymbol{\Phi}_n$ results in the following equation.

$$\left.\frac{\partial J}{\partial\boldsymbol{\Phi}_n}\right|_{\boldsymbol{\Phi}_n=\widehat{\boldsymbol{\Phi}}_n} = 0$$
$$\Rightarrow \left(\left\{\sum_{i=1}^{N_s}\boldsymbol{\Gamma}_{oi}^T\left(r_{ni}^{-2}\mathbf{H}_{\widehat{\phi}_{ni}} + 2\alpha_{ni}\mathbf{I}_{N_i}\right)\boldsymbol{\Gamma}_{oi}\right\} + \boldsymbol{\Omega}_n^T S_{\widehat{\varepsilon}_n}^{-1}\boldsymbol{\Omega}_n\right)\widehat{\boldsymbol{\Phi}}_n - 2\beta_n\widehat{\boldsymbol{\Phi}}_n + \sum_{i=1}^{N_s}r_{ni}^{-1}\boldsymbol{\Gamma}_{oi}^T H_{\widehat{\phi}_{ni}}\widehat{\boldsymbol{\phi}}_{ni} = 0 \tag{22}$$

Due to the fact that $\widehat{\boldsymbol{\phi}}_{ni}$ is the null vector of $\mathbf{H}_{\widehat{\phi}_{ni}}$ ($\mathbf{H}_{\widehat{\phi}_{ni}}\widehat{\boldsymbol{\phi}}_{ni} = \mathbf{0}$), Eq. (22) leads to the following standard eigenvalue problem.

$$\mathbf{A}_n\widehat{\boldsymbol{\Phi}}_n = \beta_n\widehat{\boldsymbol{\Phi}}_n \tag{23}$$

$$\mathbf{A}_n = \frac{1}{2}\sum_{i=1}^{N_s}\boldsymbol{\Gamma}_{oi}^T\left(r_{ni}^{-2}\mathbf{H}_{\widehat{\phi}_{ni}} + 2\widehat{\alpha}_{ni}I_{N_i}\right)\boldsymbol{\Gamma}_{oi} + \frac{1}{2}\boldsymbol{\Omega}_n^T S_{\widehat{\varepsilon}_n}^{-1}\boldsymbol{\Omega}_n \tag{24}$$

The most probable β_n and $\boldsymbol{\Phi}_n$ can be obtained as the minimum eigenvalue and its corresponding eigenvector of $\mathbf{A}_n$, respectively. However, the calculation of Eq. (24) requires the value of r_{ni} and $S_{\widehat{\varepsilon}}$ which are initially unknown since they depend on $\boldsymbol{\Phi}_n$. As a remedy, an initial estimation for $\boldsymbol{\Phi}_n$ can be obtained as the eigenvector (for minimum eigenvalue) of the following matrix by assuming zero discrepancy between $r_{ni}^{-1}\boldsymbol{\Gamma}_{oi}\boldsymbol{\Phi}_n$ and $\widehat{\boldsymbol{\phi}}_{ni}$, setting $r_{ni} = 1$, and neglecting the modelling error.

$$\mathbf{A}_{\mathrm{no}} = \sum_{\mathrm{i}=1}^{\mathrm{N_s}} \mathbf{\Gamma}_{\mathrm{oi}}^{\mathrm{T}} \mathbf{H}_{\widehat{\phi}_{\mathrm{ni}}} \mathbf{\Gamma}_{\mathrm{oi}} \tag{25}$$

Optimal value of the Lagrange multiplier, α_{ni} can be obtained by minimizing Eq. (19) with respect to $\mathrm{r_{ni}}$, as follows.

$$\begin{aligned} &\left.\frac{\partial J}{\partial r_{ni}}\right|_{r_{ni}=\widehat{r}_{ni},\alpha_{ni}=\widehat{\alpha}_{ni}} = -\widehat{r}_{ni}^{-3}\mathbf{\Phi}_n^T\mathbf{\Gamma}_{oi}^T\mathbf{H}_{\widehat{\phi}_{ni}}\mathbf{\Gamma}_{oi}\mathbf{\Phi}_n - 2\widehat{\alpha}_{ni}\widehat{r}_{ni} = 0 \\ &\Rightarrow \widehat{\alpha}_{ni} = -\frac{\widehat{r}_{ni}^{-4}}{2}\mathbf{\Phi}_n^T\mathbf{\Gamma}_{oi}^T\mathbf{H}_{\widehat{\phi}_{ni}}\mathbf{\Gamma}_{oi}\mathbf{\Phi}_n; \quad \widehat{r}_{ni}^2 = \mathbf{\Phi}_n^T\mathbf{\Gamma}_{oi}^T\mathbf{\Gamma}_{oi}\mathbf{\Phi}_n \end{aligned} \tag{26}$$

3.4.2. MPV of model parameters

MPV of model parameters ($\boldsymbol{\theta}$ and $\boldsymbol{\rho}$) can also be obtained by minimization of Eq. (19). In the previous two-stage Bayesian method by Au and Zhang [36], the prior distributions for $\boldsymbol{\theta}$ and $\boldsymbol{\rho}$ are considered as non-informative, and therefore, they are eliminated in the derivation of posterior PDF. This elimination makes it necessary to use a minimization algorithm in the maximum likelihood estimation. Defining proper prior distributions for $\boldsymbol{\theta}$ and $\boldsymbol{\rho}$, however, results in a robust minimization procedure. Thus, the MPVs of $\boldsymbol{\theta}$ and $\boldsymbol{\rho}$ can be easily obtained in a closed form solution by taking the first order derivatives of Eq. (19).

Taking the first order derivative of Eq. (19) with respect to $\boldsymbol{\theta}$ yields;

$$\begin{aligned} &\left.\frac{\partial \mathrm{J}}{\partial \boldsymbol{\theta}}\right|_{\boldsymbol{\theta}=\widehat{\boldsymbol{\theta}}} = 0 \quad \Rightarrow \widehat{\boldsymbol{\theta}}\mathrm{S}_{\widehat{\theta}_o}^{-1} - \widehat{\boldsymbol{\theta}}_0\mathrm{S}_{\widehat{\theta}_o}^{-1} + \sum_{\mathrm{n}=1}^{\mathrm{N_m}} \mathrm{S}_{\widehat{\varepsilon}}^{-1}\mathbf{G}_{\mathrm{K_n}}^{\mathrm{T}}\mathbf{G}_{\mathrm{K_n}}\widehat{\boldsymbol{\theta}} - \sum_{\mathrm{n}=1}^{\mathrm{N_m}} \mathrm{S}_{\widehat{\varepsilon}}^{-1}\mathbf{G}_{\mathrm{K_n}}^{\mathrm{T}}\mathbf{g}_{\mathrm{K_n}} = 0 \\ &\Rightarrow \widehat{\boldsymbol{\theta}} = \left[\mathrm{S}_{\widehat{\theta}_o}^{-1}\mathrm{I}_{\mathrm{N}_\theta} + \sum_{\mathrm{n}=1}^{\mathrm{N_m}} \mathrm{S}_{\widehat{\varepsilon}}^{-1}\mathbf{G}_{\mathrm{K_n}}^{\mathrm{T}}\mathbf{G}_{\mathrm{K_n}}\right]^{-1} \times \left[\widehat{\boldsymbol{\theta}}_0\mathrm{S}_{\widehat{\theta}_o}^{-1} + \sum_{\mathrm{n}=1}^{\mathrm{N_m}} \mathrm{S}_{\widehat{\varepsilon}}^{-1}\mathbf{G}_{\mathrm{K_n}}^{\mathrm{T}}\mathbf{g}_{\mathrm{K_n}}\right] \end{aligned} \tag{27}$$

where

$$\mathrm{G}_{\mathrm{K_n}} = \left[\mathbf{K}_1\mathbf{\Phi}_{\mathrm{n}} \quad \ldots \quad \mathbf{K}_{\mathrm{N}_\theta}\mathbf{\Phi}_{\mathrm{n}}\right]_{\mathrm{N}\times\mathrm{N}_\theta}; \quad \mathbf{g}_{\mathrm{K_n}} = \left[(\lambda_{\mathrm{n}}\mathbf{M}(\rho) - \mathbf{K}_0)\mathbf{\Phi}_{\mathrm{n}}\right]_{\mathrm{N}\times 1} \tag{28}$$

Similarly, minimizing Eq. (19) with respect to $\boldsymbol{\rho}$ gives the optimal mass scaling parameter vector as below.

$$\begin{aligned} &\left.\frac{\partial \mathrm{J}}{\partial \boldsymbol{\rho}}\right|_{\boldsymbol{\rho}=\widehat{\boldsymbol{\rho}}} = 0 \quad \Rightarrow \widehat{\boldsymbol{\rho}}\mathrm{S}_{\widehat{\rho}_o}^{-1} - \widehat{\boldsymbol{\rho}}_0\mathrm{S}_{\widehat{\rho}_o}^{-1} + \sum_{\mathrm{n}=1}^{\mathrm{N_m}} S_{\varepsilon}^{-1}\mathbf{G}_{\mathrm{M_n}}^{\mathrm{T}}\mathbf{G}_{\mathrm{M_n}}\widehat{\rho} - \sum_{\mathrm{n}=1}^{\mathrm{N_m}} \mathrm{S}_{\varepsilon}^{-1}\mathbf{G}_{\mathrm{M_n}}^{\mathrm{T}}\mathbf{g}_{\mathrm{M_n}} = 0 \\ &\Rightarrow \widehat{\boldsymbol{\rho}} = \left[\mathrm{S}_{\widehat{\rho}_o}^{-1}\mathrm{I}_{\mathrm{N}_\rho} + \sum_{\mathrm{n}=1}^{\mathrm{N_m}} \mathrm{S}_{\varepsilon}^{-1}\mathbf{G}_{\mathrm{M_n}}^{\mathrm{T}}\mathbf{G}_{\mathrm{M_n}}\right]^{-1} \times \left[\widehat{\boldsymbol{\rho}}_0\mathrm{S}_{\widehat{\rho}_o}^{-1} + \sum_{\mathrm{n}=1}^{\mathrm{N_m}} \mathrm{S}_{\varepsilon}^{-1}\mathbf{G}_{\mathrm{M_n}}^{\mathrm{T}}\mathbf{g}_{\mathrm{M_n}}\right] \end{aligned} \tag{29}$$

where

$$\mathbf{G}_{\mathrm{M_n}} = \lambda_{\mathrm{n}}\left[\mathbf{M}_1\mathbf{\Phi}_{\mathrm{n}} \quad \ldots \quad \mathbf{M}_{\mathrm{N}_\rho}\mathbf{\Phi}_{\mathrm{n}}\right]_{\mathrm{N}\times\mathrm{N}_\rho}; \quad \mathbf{g}_{\mathrm{M_n}} = \left[(\mathbf{K}(\boldsymbol{\theta}) - \lambda_{\mathrm{n}}\mathbf{M}_0)\mathbf{\Phi}_{\mathrm{n}}\right]_{\mathrm{N}\times 1} \tag{30}$$

Finally, the MPV of S_ε is obtained as below.

$$\begin{aligned} &\left.\frac{\partial \mathrm{J}}{\partial \mathrm{S}_\varepsilon}\right|_{\mathrm{S}_\varepsilon=\mathrm{S}_{\widehat{\varepsilon}}} = 0 \quad \Rightarrow \mathrm{S}_{\widehat{\varepsilon}}^{-1}\mathrm{N_m N} - \mathrm{S}_{\widehat{\varepsilon}}^{-2}\sum_{\mathrm{n}=1}^{\mathrm{N_m}} \mathbf{\Phi}_{\mathrm{n}}^{\mathrm{T}}\mathbf{\Omega}_{\mathrm{n}}^{\mathrm{T}}\mathbf{\Omega}_{\mathrm{n}}\mathbf{\Phi}_{\mathrm{n}} = 0 \\ &\Rightarrow \mathrm{S}_{\widehat{\varepsilon}} = \frac{\sum_{\mathrm{n}=1}^{\mathrm{N_m}} \|\mathbf{\Omega}_{\mathrm{n}}\mathbf{\Phi}_{\mathrm{n}}\|^2}{\mathrm{N_m N}} \end{aligned} \tag{31}$$

4. Summary of computational procedure

In modal parameter identification by fast BFFTA for individual setups, a norm constraint for local mode shape is necessary. Otherwise the minimization procedure becomes ill-conditioned due to the negative definite Hermitian structure of the

Hessian matrix for the local mode shape. For mode shape assembly problems, a norm constraint for global mode shape is also required to well match the identified local mode shape and corresponding part of the global mode shape. In the previous, Bayesian FE model updating applications, norm constraint for global mode shape is not necessary. If the norm constraint for $\boldsymbol{\Phi}_n$ is omitted in the presented methodology, $\mathbf{A}_{\mathrm{n}}$ will be constrained to be a semi-positive definite matrix and the most probable $\boldsymbol{\Phi}_{\mathrm{n}}$ can be obtained as the null vector of $\mathbf{A}_{\mathrm{n}}$. This case will be possible if and only if there is no modelling and measurement error, which is not expected in real applications. Therefore, the norm of $\boldsymbol{\Phi}_{\mathrm{n}}$ is constrained to unity in this study.

The flow chart for the proposed procedure is presented in Fig. 1. Here, $\boldsymbol{\lambda} = [\lambda_1 \quad \dots \quad \lambda_{N_m}]$ and $\boldsymbol{\Phi} = [\boldsymbol{\Phi}_1 \quad \dots \quad \boldsymbol{\Phi}_{N_m}]$. First, the local spectrum parameters including eigenvalues (square of most probable natural angular frequency), damping ratio, spectral density of modal excitation and prediction error should be obtained. Second, the local Hessian matrix for eigenvalues and eigenvectors (most probable local mode shape) should be obtained for each measurement setup by Gaussian approximation. At the iteration step, the posterior most probable values for model parameters are updated until the prescribed convergence criteria are satisfied.

5. Posterior uncertainty for system parameters

Posterior statistical parameters in terms of variance, standard deviation, and coefficient of variation can be estimated via the posterior covariance matrix centered at the MPV of system parameters. Using the second order Taylor series expansion, the covariance matrix can be calculated as the inverse of the Hessian matrix. Here, the Hessian matrix centered at the MPV of system parameters is given by

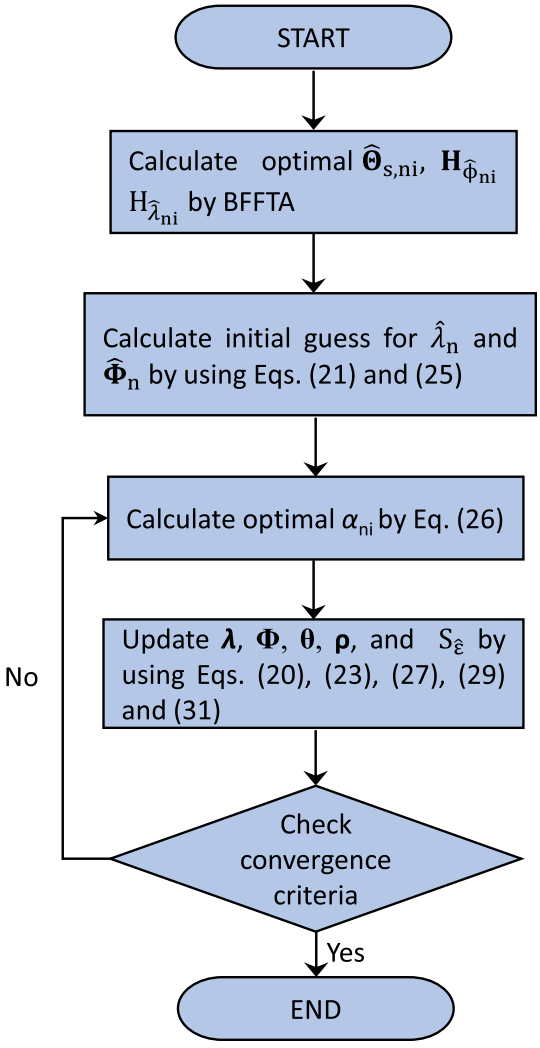

Fig. 1. Flow chart for the proposed algorithm.

$$\tilde{\mathbf{H}} = \begin{bmatrix} J^{(\theta,\theta)} & J^{(\theta,\rho)} & J^{(\theta,\lambda)} & J^{(\theta,\Phi)} \\ J^{(\rho,\theta)} & J^{(\rho,\rho)} & J^{(\rho,\lambda)} & J^{(\rho,\Phi)} \\ J^{(\lambda,\theta)} & J^{(\lambda,\rho)} & J^{(\lambda,\lambda)} & J^{(\lambda,\Phi)} \\ J^{(\Phi,\theta)} & J^{(\Phi,\rho)} & J^{(\Phi,\lambda)} & J^{(\Phi,\Phi)} \end{bmatrix}_{N_\Sigma \times N_\Sigma} \tag{32}$$

where $J^{(x,y)}$ denotes the derivatives of Eq. (19) with respect to x, and y (see Appendix B). In addition, $N_\Sigma = N_\theta + N_\rho + N_m(N+1)$. Here, Eq. ((*32*) is obtained as a singular matrix due to the unit norm constraints for $\boldsymbol{\Phi}$. Therefore, the posterior covariance matrix should be calculated by taking the pseudo inverse of the Hessian [42].

6. The probabilistic damage detection concept

The fundamental aim of FE model updating is to calibrate mathematical models of the structures. During the lifespan of a structure, it may undergo a damage after some extreme event such as an earthquake. In this case, an updated finite element model can be obtained again by using ambient vibration measurements obtained from the possibly damaged structure. Thus, it will be possible to detect the level and location of the damage by using the updated FE models for undamaged and possibly damaged cases. Here, a level of damage is defined as the change in the stiffness scaling parameters. By using Gaussian approximation for marginal distributions, Vanik et al. [43] defines the probability of exceedance of a certain damage level for the r^{th} stiffness parameter as follows.

$$P_r^{dam}(d_r) = \tilde{\Phi}\left(\frac{(1-d_r)\hat{\theta}_r^{ud} - \hat{\theta}_r^{pd}}{\sqrt{(1-d_r)^2 S_{\underset{\theta_r}{\sim}^{ud}} + S_{\underset{\theta_r}{\sim}^{pd}}}} \right) \tag{33}$$

where $d_r \in [0,\ 1]$ indicates the level of damage, $\hat{\theta}_r^{ud}$ and $\hat{\theta}_r^{pd}$ denote the most probable r^{th} stiffness scaling parameter that represents the undamaged and probably damaged cases, respectively. In addition, $S_{\underset{\theta_r}{\sim}^{ud}}$ and $S_{\underset{\theta_r}{\sim}^{pd}}$ are posterior variance of r^{th} stiffness parameter for the undamaged and damaged case, and $\tilde{\Phi}(.)$ = standard normal cumulative distribution function, respectively.

7. Numerical and experimental analysis

In this section, first a numerical analysis is presented to verify the presented procedure. For comparison purposes, the variations in the posterior uncertainties are investigated if the modelling and prediction errors are prescribed. Second, an experimental study is presented to see the effect of incomplete measurement data on the results.

In the presented methodology, both the stiffness and the mass scaling parameters are considered as model parameters to be updated. However, assuming both parameters are initially not well-estimated does not give reasonable results since an infinite number of sets for most probable stiffness and mass scaling parameters can be found. For this reason, at least one of those parameters should be assumed as well-estimated. The mass is generally much easier to be evaluated, and therefore the mass scaling parameters are assumed to be well-estimated by assigning them a small prior variance in the presented examples.

7.1. Numerical analysis: torsional shear frame

A fifteen-story torsional shear frame structure is investigated to validate the proposed methodology. The plan view of the investigated structure is presented in Fig. 2. The lateral stiffness in the x-x and y-y direction is considered as $k_{rx} = 1000$ kN/m and $k_{ry} = 600$ kN/m, respectively. In addition, story mass is $m = 250$ kg in both directions. Independent and identically distributed (*i.i.d.*) Gaussian white noise excitations are generated with 300 s duration and 100 Hz sampling frequency, and they are assigned as point forces to the mass center of the slab along translational and torsional directions, respectively. The measurement noise root mean square (*rms*) level is set to be 20% of the *rms* of the noise-free simulated response, for each channel. The structure is measured with four setups, and the sensor configuration of the setups is presented in Table 1. The acceleration responses of the structure are measured at the center in the translational directions. Torsional acceleration measurements are omitted. Therefore, torsional modes are not identified, but they are extracted from the updated finite element model.

Assuming the non-parametric stiffness and mass components are equal to zero ($\mathbf{K}_0 = 0, \mathbf{M}_0 = 0$), the parametric stiffness and mass matrices are defined as,

$$\mathbf{K}(\boldsymbol{\theta}) = \sum_{r=1}^{N_{\theta x}=15} \theta_{xr}\mathbf{K}_{xr} + \sum_{r=1}^{N_{\theta y}=15} \theta_{yr}\mathbf{K}_{yr} \tag{34}$$

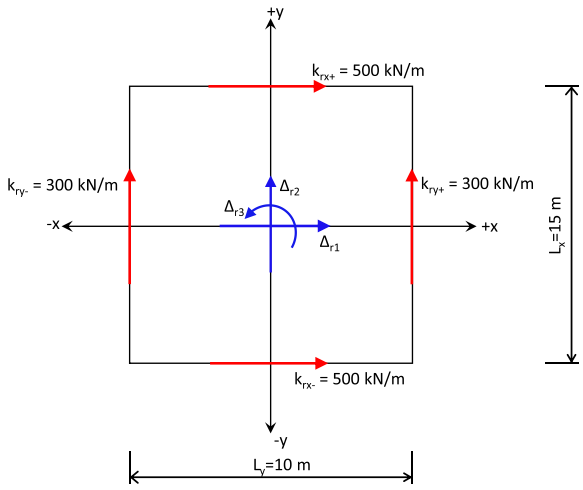

Fig. 2. Plan view (r^{th} story) of the fifteen-story torsional shear frame structure.

Table 1
Multiple setup configuration.

Setup No	Measured DOF
1	1*x*, 1*y*, 2*x*, 2*y*, 3*x*, 3*y*, 4*x*, 4*y*, 5*x*, 5*y*
2	4*x*, 4*y*, 5*x*, 5*y*, 6*x*, 6*y*, 7*x*, 7*y*, 8*x*, 8*y*
3	7*x*, 7*y*, 8*x*, 8*y*, 9*x*, 9*y*, 10*x*, 10*y*, 11*x*, 11*y*, 12*x*, 12*y*
4	11*x*, 11*y*, 12*x*, 13*y*, 13*x*, 13*y*, 14*x*, 14*y*, 15*x*, 15*y*

$$\mathbf{M}(\boldsymbol{\rho}) = \sum_{r=1}^{N\rho=15} \rho_r \mathbf{M}_r \tag{35}$$

Model parameters for the investigated structure are first updated by assuming an undamaged case which should lead to the actual stiffness scaling parameters as $\theta_{xr} = \theta_{yr} = 1.00$ (for r = 1, 2, 3, … ,15). Next, a damaged case is considered in which the inter-story stiffnesses in x-x direction are reduced by 30% in the first story and by 60% in the seventh story. Further, the inter-story stiffnesses in y-y direction are reduced by 10% in the second story and by 25% in the fifth story. In this damaged case, the stiffness scaling parameters are expected to be evaluated as $\theta_{x1} = 0.70$, $\theta_{x7} = 0.40$, $\theta_{y2} = 0.90$, $\theta_{y5} = 0.75$ and the remaining stiffness scaling parameters should be 1.00.

The prior most probable values for stiffness parameters are selected as $\theta_{xr0} = \theta_{yr0} = 10$ (overestimated) with a variance of $S_{\theta 0} = 50$. In addition, the prior mass parameters are assumed to be well-estimated with $\rho_{ro} = 1$ and $S_{\rho 0} = 0.01$. The resulting prior probability distributions for stiffness and mass scaling parameters are presented in Fig. 3.

The updated natural frequencies for the first fifteen modes are presented in Table 2. Here, the translational modes indicate the identified most probable values by using the presented algorithm. The torsional modes, however, are not measured in the considered example. Therefore, their modal parameters cannot not be identified. Instead, the system modal parameters for torsional modes are obtained from the eigenvalue analysis of the updated finite element model. It is seen that the identified frequencies match well with their actual values. In addition, the identified stiffness scaling parameters and the corresponding posterior coefficient of variations (c.o.v.) in the x-x and y-y directions are presented in Tables 3 and 4, respectively. Again, a well-match is observed between the identified and actual stiffness scaling parameters, for both the undamaged and the damaged cases.

In the literature, the modelling and prediction errors are generally defined as rigid constraints (they are assigned to the selected prescribed values) which may not reflect the actual case. The presented method, however, defines soft constraints for modelling and prediction errors. Therefore, the possible discrepancies due to the modelling and prediction error are updated at each iteration step. Fig. 4 presents the cumulative probability density functions for damage with respect to the possible damage levels. It is seen that the probabilities of damage show very small (nearly zero) variance around the most probable damage levels. The reason of this fact is thought to be the result of using soft constraints for the modelling and prediction error.

Some applications in the literature consider the measured eigenvalues as the prescribed values (rigid constraint) and the possible prediction errors are neglected [1,44]. For the rigid constraint case, $\boldsymbol{\lambda}$ is set to the MPVs that are identified from the

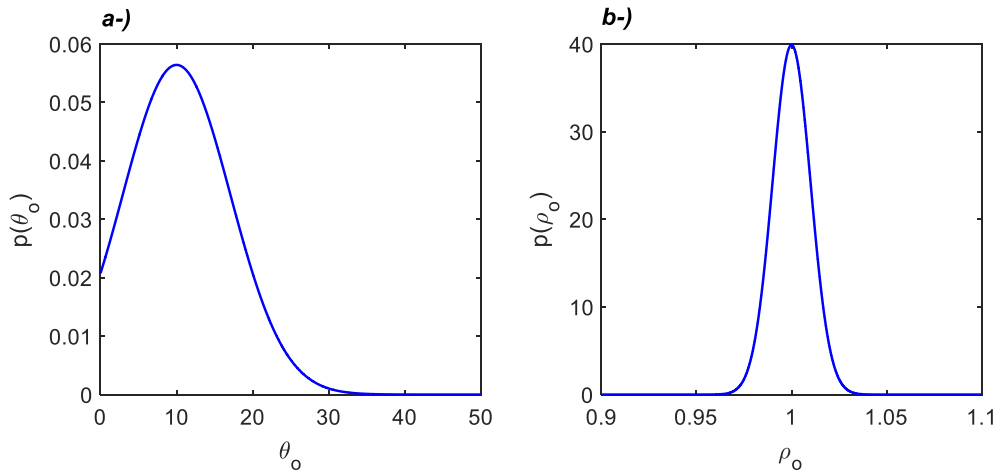

Fig. 3. Prior probability distributions of (a) stiffness and (b) mass scaling parameters.

Table 2
Actual and updated natural frequencies with posterior c.o.v.

Mode Number	Undamaged Case				Damaged Case			
	Dir.	Actual (Hz.)	Updated (Hz.)	*c.o.v.* ($\times 10^{-10}$)	Dir.	Actual (Hz.)	Updated (Hz.)	*c.o.v.* ($\times 10^{-10}$)
1	*y*	0.79	0.79	0.22	*y*	0.77	0.77	4.68
2	*x*	1.02	1.02	0.33	*x*	0.94	0.94	3.48
3	*Tors*	1.50	1.50*	–	*Tors*	1.45	1.45*	–
4	*y*	2.36	2.37	0.15	*y*	2.36	2.36	2.60
5	*x*	3.05	3.05	0.26	*x*	2.91	2.92	2.30
6	*y*	3.91	3.92	0.08	*y*	3.87	3.86	1.42
7	*Tors*	4.49	4.50*	–	*x*	4.55	4.56	1.10
8	*x*	5.04	5.04	0.11	*Tors*	4.42	4.41*	–
9	*y*	5.42	5.42	0.03	*y*	5.28	5.28	1.01
10	*y*	6.87	6.86	0.01	*y*	6.78	6.78	0.72
11	*x*	6.99	6.99	0.05	*x*	6.84	6.84	0.83
12	*Tors*	7.43	7.43*	–	*Tors*	7.18	7.18*	–
13	*x*	8.87	8.87	0.02	*x*	8.19	8.20	0.61
14	*Tors*	10.29	10.29*	–	*Tors*	10.08	10.08*	–
15	*Tors*	13.06	13.07*	–	*Tors*	12.61	12.60*	–

Table 3
Actual and updated stiffness parameters in the x-x direction.

Parameter	Undamaged case			Damaged case		
	Actual	Updated	*c.o.v* ($\times 10^{-14}$)	Actual	Updated	*c.o.v* ($\times 10^{-14}$)
θ_{x1}	1.0000	1.0044	1.0214	0.7000	0.7078	8.4405
θ_{x2}	1.0000	1.0114	1.2943	1.0000	1.0107	10.8562
θ_{x3}	1.0000	1.0076	0.8476	1.0000	1.0059	8.6016
θ_{x4}	1.0000	1.0089	1.0702	1.0000	1.0114	8.3922
θ_{x5}	1.0000	1.0089	1.0193	1.0000	1.0062	7.7128
θ_{x6}	1.0000	1.0056	1.0326	1.0000	1.0043	6.9394
θ_{x7}	1.0000	1.0109	1.0056	0.4000	0.4009	2.3786
θ_{x8}	1.0000	1.0010	1.0221	1.0000	1.0076	5.9229
θ_{x9}	1.0000	1.0168	0.9642	1.0000	1.0074	6.5112
θ_{x10}	1.0000	1.0000	0.7876	1.0000	1.0029	8.5295
θ_{x11}	1.0000	1.0057	0.8855	1.0000	1.0037	5.7305
θ_{x12}	1.0000	0.9991	1.0363	1.0000	1.0090	10.6522
θ_{x13}	1.0000	1.0076	1.0826	1.0000	1.0100	7.9952
θ_{x14}	1.0000	1.0125	0.7692	1.0000	1.0016	11.6128
θ_{x15}	1.0000	0.9987	0.9038	1.0000	1.0003	14.9658

measurements [45]. In this study, however, the prediction error between the system and measured eigenvalues are considered as parameters to be updated. Fig. 5 and Fig. 6 show the convergence speed of the estimated first stiffness scaling parameter to its actual value and the variation of its posterior c.o.v. with respect to the number of considered modes, for the cases of rigid and soft constraints for $\boldsymbol{\lambda}$, respectively. It is seen that the presented methodology (soft constraint approach)

Table 4
Actual and updated stiffness parameters in the y-y direction.

Parameter	Undamaged case			Damaged case		
	Actual	Updated	*c.o.v* ($\times 10^{-14}$)	Actual	Updated	*c.o.v* ($\times 10^{-14}$)
θ_{y1}	1.0000	1.0090	1.4566	1.0000	1.0035	11.2068
θ_{y2}	1.0000	1.0105	1.0229	0.9000	0.9089	9.7372
θ_{y3}	1.0000	1.0133	0.9693	1.0000	1.0079	12.1623
θ_{y4}	1.0000	0.9973	0.7562	1.0000	0.9944	15.5966
θ_{y5}	1.0000	1.0085	1.2633	0.7500	0.7521	8.7421
θ_{y6}	1.0000	1.0027	1.0756	1.0000	0.9971	6.4256
θ_{y7}	1.0000	1.0021	1.5264	1.0000	1.0005	5.9322
θ_{y8}	1.0000	1.0105	1.0523	1.0000	1.0014	4.3256
θ_{y9}	1.0000	1.0070	0.9145	1.0000	1.0105	7.1385
θ_{y10}	1.0000	1.0091	1.1580	1.0000	1.0158	9.9661
θ_{y11}	1.0000	1.0137	1.6386	1.0000	1.0144	11.1286
θ_{y12}	1.0000	0.9973	1.1325	1.0000	0.9957	12.5625
θ_{y13}	1.0000	1.0093	1.4086	1.0000	0.9989	8.4346
θ_{y14}	1.0000	0.9982	0.9373	1.0000	1.0085	10.0628
θ_{y15}	1.0000	1.0070	1.1548	1.0000	0.9924	12.0963

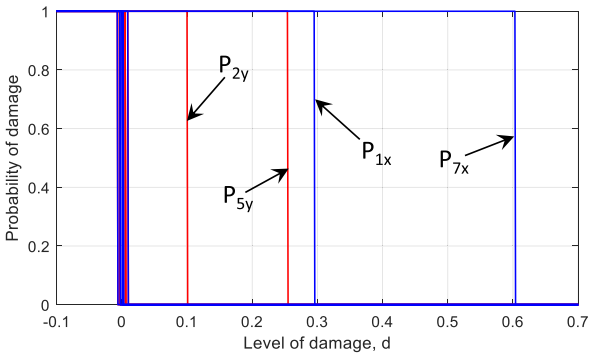

Fig. 4. Probability of damage for the stiffness parameters (blue line: x-x direction, red line: y-y direction).

increases the convergence speed of the estimated stiffness parameters to the actual value when compared to the rigid constraint approach. In addition, the presented methodology significantly reduces the posterior c.o.v. for the first stiffness scaling parameter.

Fig. 7 and Fig. 8 show the variation of the estimated first stiffness scaling parameter and its posterior c.o.v. for the prescribed variance of modelling and measurement error. Here, the prediction error for eigenvalues and eigenvectors were

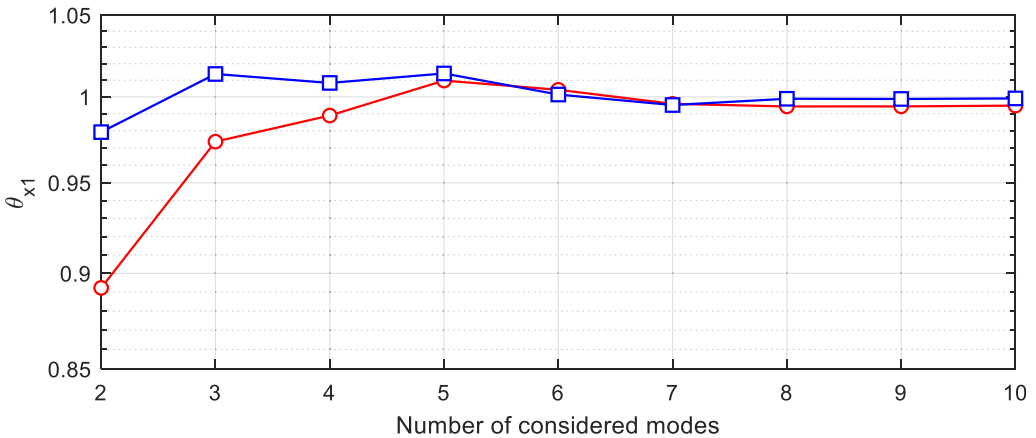

Fig. 5. Variation of estimated θ_{x1} versus the number of considered modes (red circle: rigid constraint, blue square: soft constraint for eigenvalues). (For interpretation of the references to colour in this figure legend, the reader is referred to the Web version of this article.)

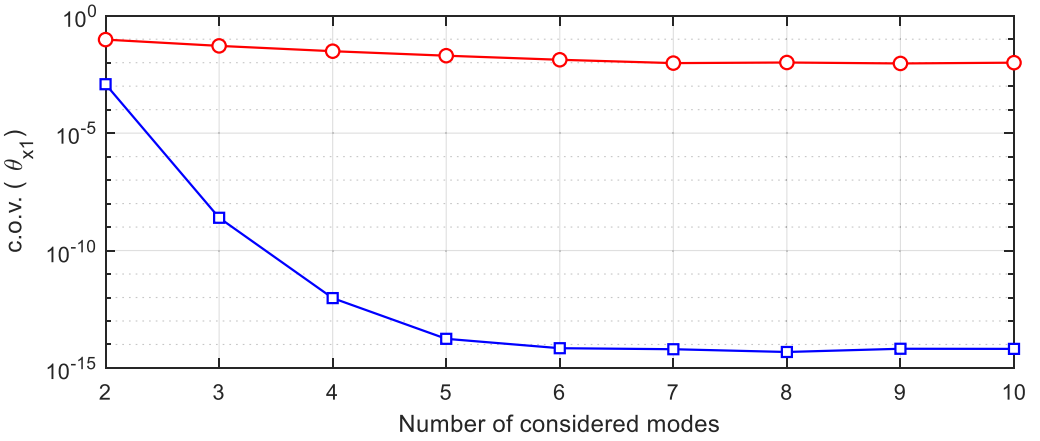

Fig. 6. Variation of posterior c.o.v. of θ_{x1} versus the number of considered modes (red circle: rigid constraint, blue square: soft constraint for eigenvalues).

defined to have a c.o.v. of 1%. The prescribed variance of modelling error was calculated according to the defined prediction error. When the modelling error level is prescribed, the posterior uncertainties are affected by the chosen value even if the identified MPVs for model parameters are close to the actual value. The definition of smaller error values does not guarantee a smaller posterior c.o.v. for model parameters. In addition, some applications completely neglect the modelling error which may also result in larger posterior uncertainty [36–38]. Results show that the soft constraint approach for modelling and measurement error increases the convergence speed of most probable stiffness scaling parameters and shows a significant decrease in the posterior coefficient of variation.

Fig. 9 and Fig. 10 show the updated first fifteen mode shapes for the damaged and undamaged cases. Here, the torsional mode shapes were estimated from the updated FE model. The estimated mode shapes (presented by blue squares) match well with the analytical results for both undamaged and damaged cases. In addition, the posterior c.o.v. values for the identified mode shapes are presented in Table 5.

In order to see the effect of measurement noise on the FE model updating results, the damaged case for the considered structure is investigated with respect to different noise levels. Here, the noise level is defined as the ratio of the *rms* values of the noise and noise-free response. Fig. 11 presents the variations of the relative error between the most probable and actual eigenvalues for the first three modes, and the posterior c.o.v. values with respect to noise level. Maximum error increases up to 1% for the noise level of 100%. Posterior c.o.v. values show significant variation. However, their maximums remain in the level of 10^{-8}. In addition, Fig. 12 presents the variations of the relative error between the most probable and actual stiffness scaling parameters, and their posterior c.o.v. values with respect to noise level. A similar trend is observed in the results for the stiffness scaling parameters. It is seen that the relative error shows a reasonable increase for the larger noise levels. A

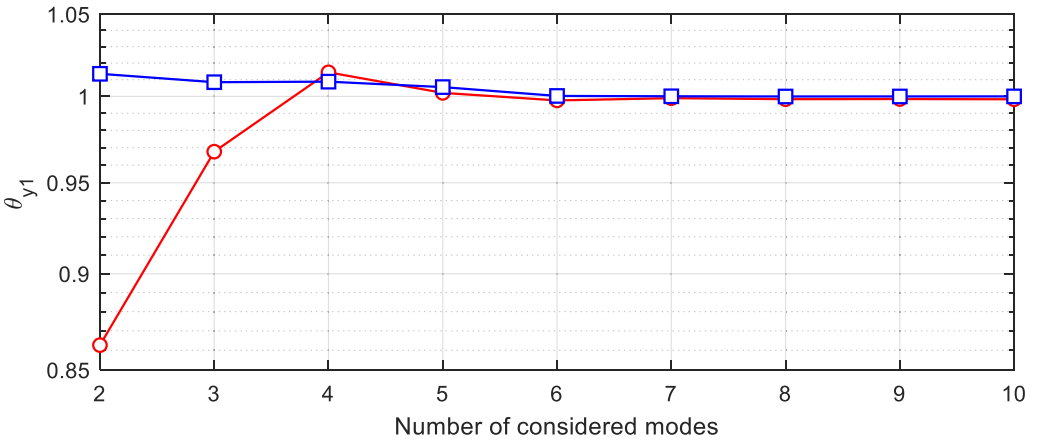

Fig. 7. Variation of posterior c.o.v. versus the number of considered modes (red circle: rigid constraint, blue square: soft constraint for modelling and prediction error).

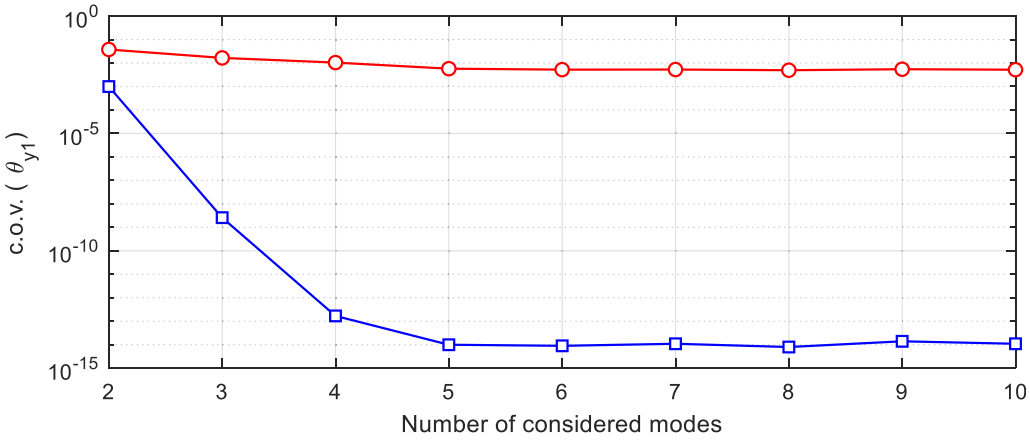

Fig. 8. Variation of posterior c.o.v. of θ_{y1} versus the number of considered modes (red circle: rigid constraint, blue square: soft constraint for modelling and prediction error).

significant increase is observed for the posterior uncertainties, but its maximum value also remains in a considerably small level.

7.2. Experimental analysis: ten story shear frame model

In this section, the presented methodology is applied to a ten-story laboratory shear frame whose schematic representation is presented in Fig. 13. In the laboratory experiments, four piezo-electric accelerometers were used which are defined with 1000 mV/g sensitivity and 11.4 μg/(Hz.)$^{0.5}$ spectral noise density. The measurement system consists of a laptop computer with a 1.5 GHz single CPU and Linux operating system, a 16 channel USBDUX-Sigma data acquisition box with 24 bit analog to digital conversion. A first order analog lowpass filter with a cut-off frequency at 120 Hz, and a constant current supply was used for each channel.

In order to shed light on the effect of incomplete measurement data onto the FE model updating results, three different scenarios were considered. First, the structure was measured with four accelerometers in four setups, covering all DOF (Fig. 13d). Next, the measurement scenarios were created by the selection of measurement channels according to Table 6. As it can be observed, the number of measured channels increases from Scenario-I to III. The acceleration responses were recorded in the weak direction of the building and all measurement setups were acquired in different times with 250 Hz sampling frequency and 5 min duration.

The inter-story stiffnesses of the structure were analytically calculated as [37.50 37.50 37.50 25.00 25.00 25.00 25.00 18.75 18.75 18.75] KN/m according to the structural geometrical configuration and assumed material property. In addition, the story mass was calculated as 2.355 kg for each story. For real life applications in which the nominal stiffness parameters are assumed to be well estimated, one may take a prior estimation of 1.00. In this study, however, the prior estimation for stiffness scaling parameters were intentionally considered as overestimated and assigned to 10.0 with a large variance. The prior mass scaling parameters were selected as 1.00 with small variance (well-estimated).

Table 7 presents the identified MPVs of natural frequencies and their posterior c.o.v. values. Here, "MPV*" denotes the most probable frequencies identified by BFFTA, and "MPV" denotes the most probable frequencies identified by using the presented Bayesian FE model updating approach. Results show that the discrepancy between the updated and measured values are very small. In addition, as the number of measured DOF increases, MPVs and their posterior c.o.v. for eigenvalues show no significant changes.

Identified stiffness parameters and their posterior c.o.v. values are presented in Table 8. At first view, it is seen that the identified stiffness parameters show a maximum difference of about 7% among Scenario-I and III. This difference is considered to be caused by the effect of insufficient measurement points in Scenario-I. Here, only the first five modes could be identified by the presented method, because five DOFs were measured only. The absence of higher modes results in a relatively weaker estimation for stiffness parameters. The results from Scenario II show a small difference from Scenario III, since only the last two modes out of ten were not considered. In addition, the posterior c.o.v. shows significant increase in case of insufficient measurement points. Despite, a maximum relative difference of 7% in the stiffness parameters, the posterior most probable mode shapes are observed to be identical for the considered scenarios (see Fig. 14).

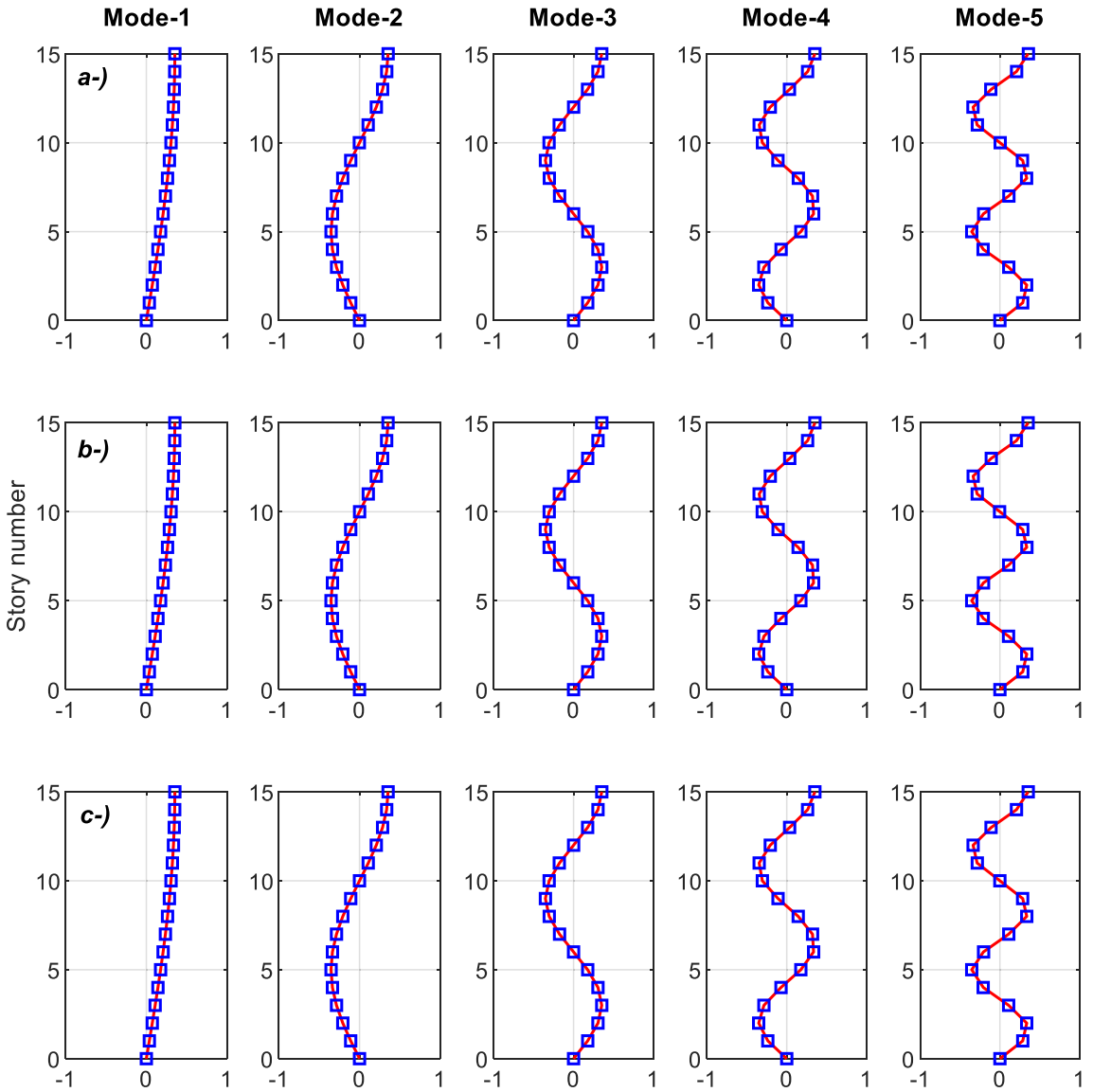

Fig. 9. Updated mode shapes (blue square) and analytical values (red line) for undamaged case: a-) y-y direction, b-) x-x direction, and c-) torsional.

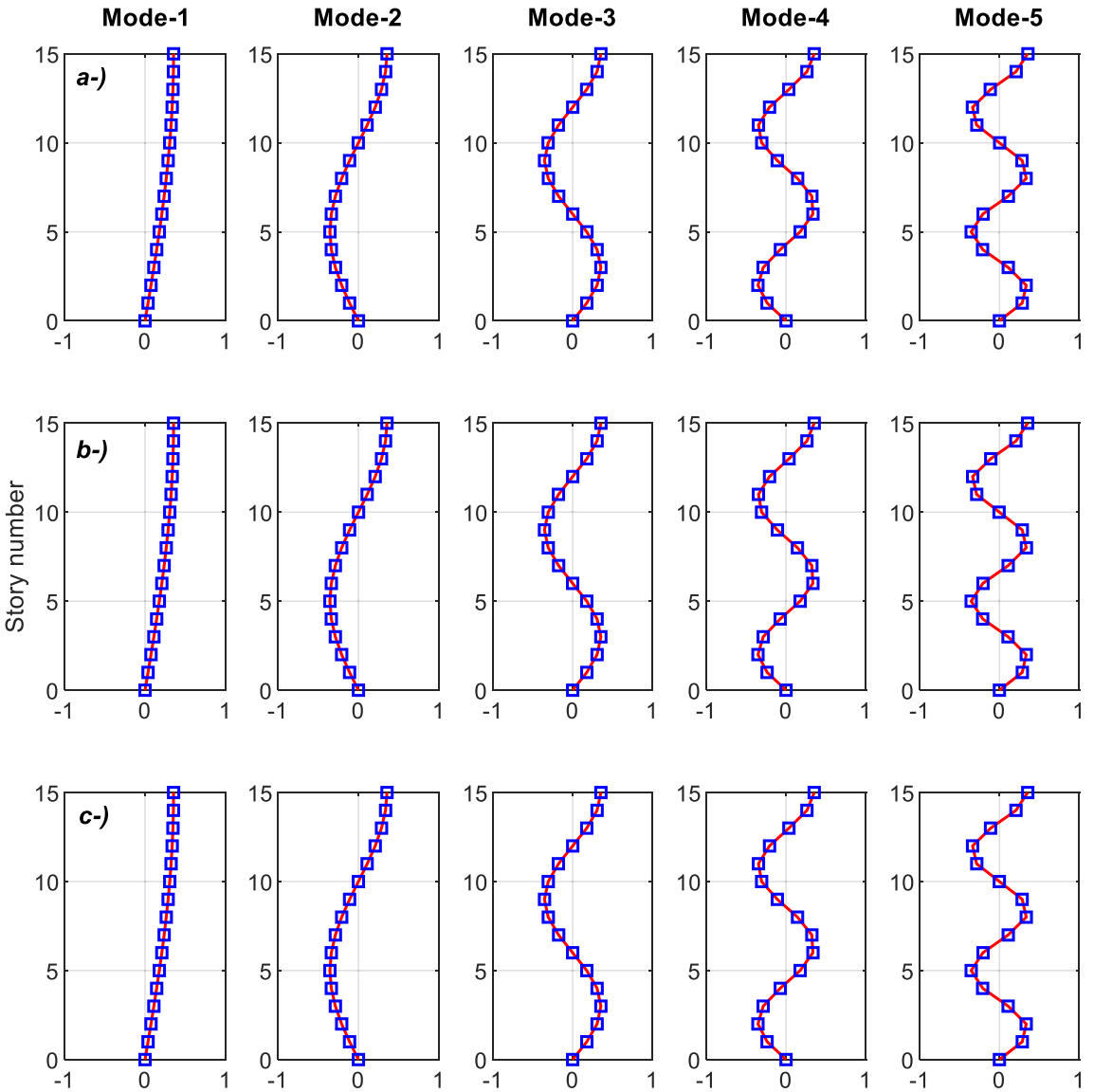

Fig. 10. Updated mode shapes (blue square) and analytical values (red line) for damaged case: a-) y-y direction, b-) x-x direction, and c-) torsional.

Table 5
Posterior c.o.v. values for updated most probable mode shapes ($\times 10^{-12}$).

Mode number	Undamaged case		Damaged case	
	yy-dir	xx-dir.	yy-dir	xx-dir.
1	3.86	4.25	57.35	69.93
2	5.25	4.92	77.42	91.16
3	5.85	6.04	89.83	103.25
4	7.23	8.23	110.21	123.86
5	9.16	9.95	132.36	145.79

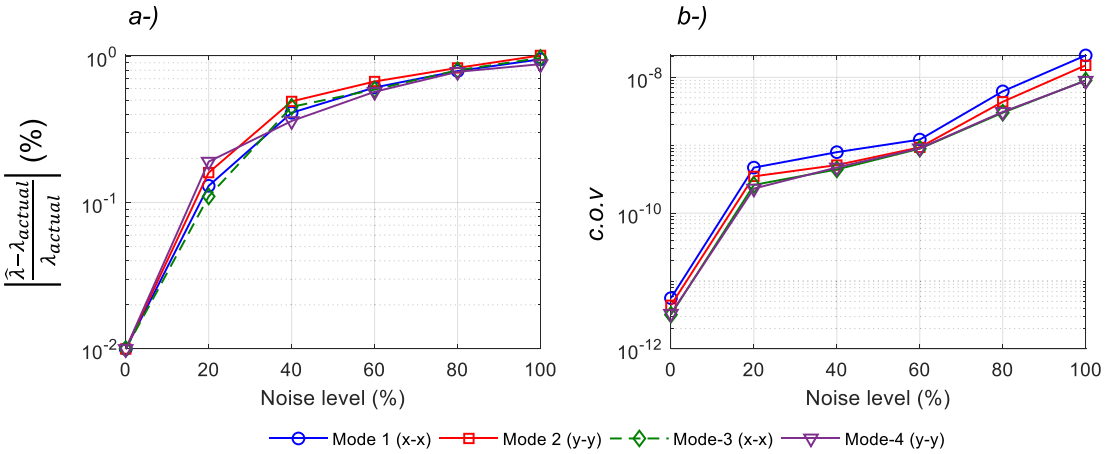

Fig. 11. a-) Variation of relative error ratio (%) in eigenvalues with respect to noise level, and b-) variation of posterior c.o.v. of updated eigenvalues with respect to noise level.

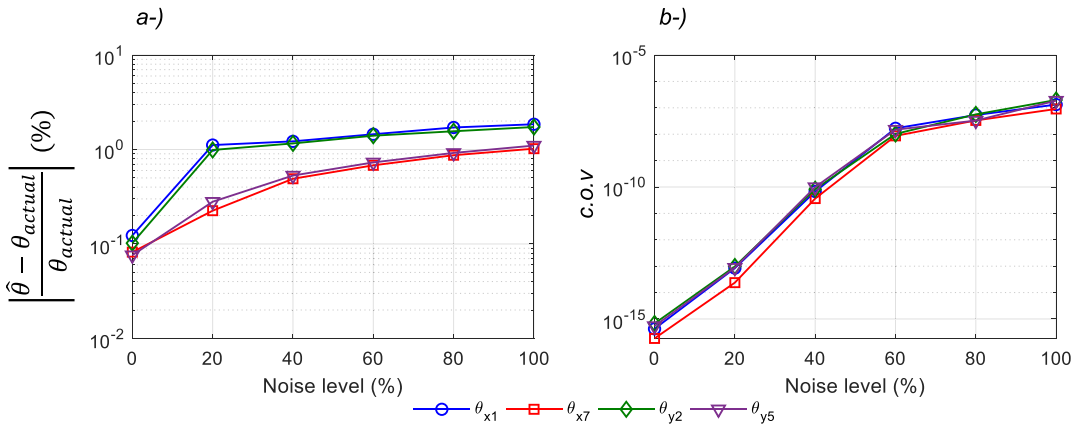

Fig. 12. a-) Variation of relative error (%) in updated stiffness scaling parameters with respect to noise level, and b-) variation of posterior c.o.v. of updated stiffness scaling parameters with respect to noise level.

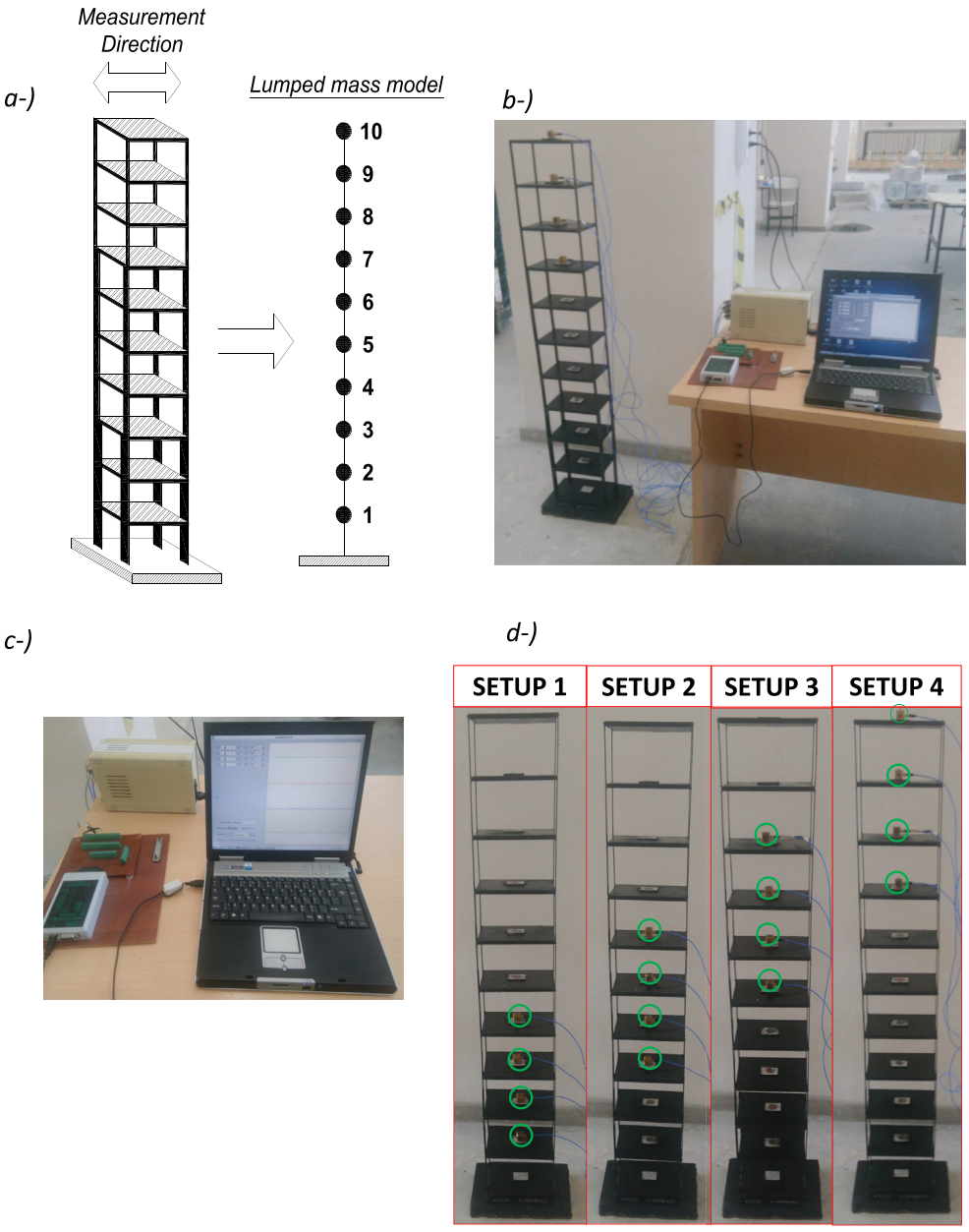

Fig. 13. a-) Schematic view of ten story shear frame structure, b-) view of the whole experimental setup, c-) data acquisition system, and d-) multiple setups configuration (for scenario III).

Table 6
Sensor placement for considered measurement scenarios.

Setup Number	Measured DOFs		
	Scenario I	Scenario II	Scenario III
1	1, 4	2, 3, 4	1, 2, 3, 4
2	4, 6	4, 5, 6	3, 4, 5, 6
3	6, 8	5, 6, 7	5, 6, 7, 8
4	8, 10	7, 9, 10	7, 8, 9, 10

Table 7
MPVs and posterior c.o.v. for natural frequencies ("*" denotes the MPVs that are identified from the measurements by BFFTA).

Mode #	Scenario I			Scenario II			Scenario III		
	MPV*	MPV	c.o.v (%)	MPV*	MPV	c.o.v (%)	MPV*	MPV	c.o.v (%)
1	2.61	2.62	0.11	2.62	2.62	0.08	2.62	2.62	0.07
2	7.36	7.37	0.06	7.37	7.37	0.05	7.37	7.37	0.05
3	11.67	11.69	0.03	11.69	11.69	0.01	11.70	11.70	0.01
4	17.02	17.03	0.02	17.03	17.03	0.01	17.03	17.03	0.01
5	20.72	20.70	0.02	20.72	20.71	0.01	20.71	20.71	0.01

Table 8
Identified stiffness scaling parameters for considered measurement scenarios.

Stiffness Parameter	Scenario I		Scenario II		Scenario III	
	MPV	c.o.v (%)	MPV	c.o.v (%)	MPV	c.o.v (%)
θ_1	0.9544	0.3195	0.9916	0.2927	1.0154	0.1607
θ_2	0.9226	0.5147	0.8902	0.3729	0.8875	0.1700
θ_3	0.9839	0.5701	0.9544	0.1484	0.9448	0.1025
θ_4	1.1517	0.5723	1.0961	0.1512	1.1135	0.1015
θ_5	0.9515	0.6093	1.0239	0.1944	1.0278	0.1288
θ_6	1.0957	0.7114	1.0484	0.2180	1.0524	0.1497
θ_7	1.1495	0.5564	1.1989	0.1774	1.1805	0.1177
θ_8	1.1001	0.7402	1.0897	0.2214	1.0849	0.1311
θ_9	1.0020	0.6004	1.0379	0.2192	1.0497	0.1314
θ_{10}	1.0596	0.5782	1.0316	0.2170	1.0443	0.1343

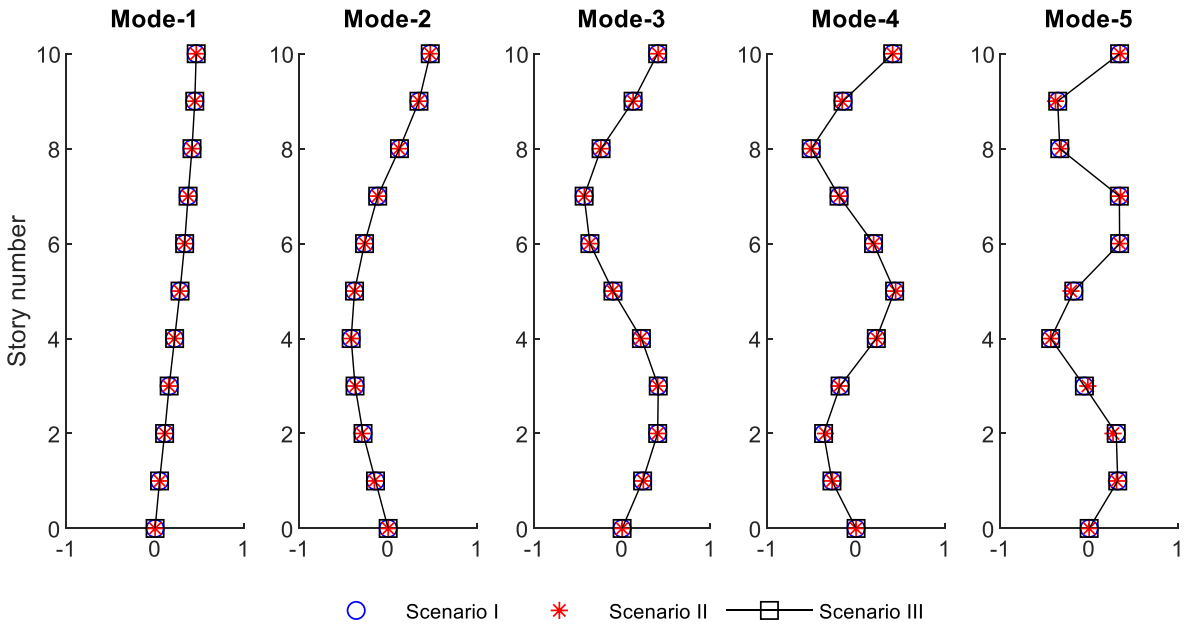

Fig. 14. Updated mode shapes for considered scenarios.

8. Conclusion

Motivated from the literature, this study presents a two-stage Bayesian finite element model updating procedure by using the acceleration response obtained by multiple setups from ambient excitations. The main difference from the previous studies stands on consideration of the prediction and modelling error terms. In the modal identification stage, BFFTA is employed to the finite element model updating problem to quantify the prediction error term. A block diagonal covariance matrix is obtained which indicates a zero-correlation between the eigenvalues and eigenvectors. Thus, a prior probability distribution for the prediction error between the most probable and measured eigenvalues and eigenvectors are obtained for each measurement setup. Finally, the posterior MPVs for model and system modal parameters are updated by using Bayes' theorem. Numerical and experimental studies are presented to see the efficiency of the proposed methodology.

The proposed procedure results in lower posterior uncertainty when compared to the rigid constraint approach for modelling and prediction error. The reason of this fact is considered to stem from using the posterior distribution of local modal parameters obtained by BFFTA at each setup for prior probability distribution of eigenvalues and eigenvectors together with the modelling error. Using a prescribed prediction error or neglecting the prediction error for eigenvalues results in significant increase in the posterior uncertainty. Additionally, in case of multiple measurement setups and/or insufficient measurement points, the presented methodology gives reasonable results for system parameters.

Appendix A

Calculation of Hessian matrix for local modal parameters

The Hessian matrix for the nth mode local modal parameters at i^{th} measurement setup can be calculated by following a fast-computational procedure that is proposed by Au and Xie [40]. In this procedure, a constrained likelihood function, $L_{c,ni}(\boldsymbol{\Theta}_{ni})$ with one independent mode shape equality constraint (for n^{th} mode and i^{th} setup) is considered as below.

$$L_{c,ni}(\boldsymbol{\Theta}_{ni}) = L_{ni}(\boldsymbol{\Theta}_{ni}) + \overline{\alpha}_{j,ni} G_{j,ni} \tag{A.1}$$

Here, $\overline{\alpha}_{j,ni}$ and $G_{j,ni}$ denote the Lagrange multipliers and constraint equations. The Hessian matrix with respect to $\boldsymbol{\Theta}_{ni}$ is obtained as,

$$\nabla^2 L_{c,ni} = \nabla \mathbf{v}_c^T \left(\nabla^2 L_{ni} + \overline{\alpha}_{j,ni} \nabla^2 G_{j,ni} \right) \nabla \mathbf{v}_c \tag{A.2}$$

where $\mathbf{v}_c$ denotes a mapping function that always satisfies the constraint equations. The second order derivative of the likelihood function is given by

$$\nabla^2 L_{ni} = \nabla^2 L_{ni}(\boldsymbol{\Theta}_{ni})\Big|_{\boldsymbol{\Theta}_{ni}=\mathbf{v}_c(\boldsymbol{\Theta}_{ni})} = \nabla^2 \begin{bmatrix} L_{ni}^{(\boldsymbol{\Theta}_{sni},\boldsymbol{\Theta}_{sni})} & L_{ni}^{(\boldsymbol{\Theta}_{sni},\phi_{ni})} \\ L_{ni}^{(\phi_{ni},\boldsymbol{\Theta}_{sni})} & L_{ni}^{(\phi_{ni},\phi_{ni})} \end{bmatrix} \tag{A.3}$$

where $\mathbf{v}_c$, G_i and their derivatives are written as below.

$$\begin{aligned} &\boldsymbol{\Theta} = \begin{bmatrix} \boldsymbol{\Theta}_{sni} \\ \phi_{ni} \end{bmatrix}; \qquad \mathbf{v}_c(\boldsymbol{\Theta}_{ni}) = \begin{bmatrix} \boldsymbol{\Theta}_{sni} \\ \dfrac{\phi_{ni}}{\|\phi_{ni}\|} \end{bmatrix}; \qquad G_i = \phi_{ni}^T \phi_{ni} - 1; \\ &\nabla \mathbf{v}_c = \begin{bmatrix} \mathbf{I}_{4\times 4} & \mathbf{0}_{4\times N_i} \\ \mathbf{0}_{N_i\times 4} & \mathbf{I}_N - \phi_{ni}\phi_{ni}^T \end{bmatrix}; \quad \nabla^2 G_i = \begin{bmatrix} \mathbf{0}_{4\times 4} & \mathbf{0}_{4\times N_i} \\ \mathbf{0}_{N_i\times 4} & 2\mathbf{I}_{N_i} \end{bmatrix} \end{aligned} \tag{A.4}$$

Thus, the Hessian matrix under norm constraint is obtained as follows

$$\nabla^2 L_{c,ni} = \begin{bmatrix} \mathbf{I}_{4\times 4} & \mathbf{0}_{4\times N_i} \\ \mathbf{0}_{N_i\times 4} & \mathbf{I}_N - \phi_{ni}\phi_{ni}^T \end{bmatrix} \nabla^2 \begin{bmatrix} L_{\boldsymbol{\Theta}_{sni}\boldsymbol{\Theta}_{sni}} & L_{\boldsymbol{\Theta}_{sni}\phi_{ni}} \\ L_{\phi_{ni}\boldsymbol{\Theta}_{sni}} & L_{\phi_{ni}\phi_{ni}} + 2\overline{\alpha}_{ni}\mathbf{I}_{N_i} \end{bmatrix} \begin{bmatrix} \mathbf{I}_{4\times 4} & \mathbf{0}_{4\times N_i} \\ \mathbf{0}_{N_i\times 4} & \mathbf{I}_N - \phi_{ni}\phi_{ni}^T \end{bmatrix} = \begin{bmatrix} \nabla^2 L_{c,ni}^{(\boldsymbol{\Theta}_{sni},\boldsymbol{\Theta}_{sni})} & \nabla^2 L_{c,ni}^{(\boldsymbol{\Theta}_{sni},\phi_{ni})} \\ \nabla^2 L_{c,ni}^{(\phi_{ni},\boldsymbol{\Theta}_{sni})} & \nabla^2 L_{c,ni}^{(\phi_{ni},\phi_{ni})} \end{bmatrix} \tag{A.5}$$

where

$$\begin{aligned}
&\nabla^2 L_{c,ni}^{(\boldsymbol{\Theta}_{sni},\boldsymbol{\Theta}_{sni})} = \nabla^2 L_{ni}^{(\boldsymbol{\Theta}_{sni},\boldsymbol{\Theta}_{sni})} \\
&\nabla^2 L_{c,ni}^{(\boldsymbol{\Theta}_{sni},\boldsymbol{\phi}_{ni})} = \nabla^2 L_{ni}^{(\boldsymbol{\Theta}_{sni},\boldsymbol{\phi}_{ni})} \left(\mathbf{I}_N - \boldsymbol{\phi}_{ni}\boldsymbol{\phi}_{ni}^T\right) \qquad \mathbf{I}_{N_i}\left)\left(\mathbf{I}_N - \boldsymbol{\phi}_{ni}\boldsymbol{\phi}_{ni}^T\right)\right. \\
&\nabla^2 L_{c,ni}^{(\boldsymbol{\phi}_{ni},\boldsymbol{\phi}_{ni})} = \left(\mathbf{I}_N - \boldsymbol{\phi}_{ni}\boldsymbol{\phi}_{ni}^T\right)\left(\nabla^2 L_{ni}^{(\phi_{ni},\phi_{ni})} + 2\overline{\alpha}_{ni}\right. \\
&= -2\Delta_{ni} + 2\overline{\alpha}_{ni}\mathbf{I}_{N_i} - 2\boldsymbol{\phi}_{ni}\boldsymbol{\phi}_{ni}^T\Delta_{ni}\boldsymbol{\phi}_{ni}\boldsymbol{\phi}_{ni}^T + 2\boldsymbol{\phi}_{ni}\boldsymbol{\phi}_{ni}^T\overline{\alpha}_{ni}\boldsymbol{\phi}_{ni}\boldsymbol{\phi}_{ni}^T
\end{aligned} \tag{A.6}$$

At $\boldsymbol{\Theta}_{sni} = \widehat{\boldsymbol{\Theta}}_{sni}$ and $\boldsymbol{\phi}_{ni} = \widehat{\boldsymbol{\phi}}_{ni}$,

$$\begin{aligned}
\mathbf{H}_{\widehat{\boldsymbol{\Theta}}_{sni}\widehat{\boldsymbol{\phi}}_{ni}} &= \widehat{\boldsymbol{\phi}}_{ni}^T \times \frac{\partial \boldsymbol{\Delta}_{ni}}{\partial \boldsymbol{\Theta}_{sni}}\bigg|_{\boldsymbol{\Theta}_{sni}=\widehat{\boldsymbol{\Theta}}_{sni}} \times \left(\mathbf{I}_{N_i} - \widehat{\boldsymbol{\phi}}_{ni}\widehat{\boldsymbol{\phi}}_{ni}^T\right) \\
&= \widehat{\boldsymbol{\phi}}_{ni}^T \times \frac{\partial \boldsymbol{\Delta}_{ni}}{\partial \widehat{\boldsymbol{\Theta}}_{sni}}\bigg|_{\boldsymbol{\Theta}_{sni}=\widehat{\boldsymbol{\Theta}}_{sni}} \times \left(0 \times \widehat{\boldsymbol{\phi}}_{ni}\widehat{\boldsymbol{\phi}}_{ni}^T - \sum_{j=2}^{N_i} \boldsymbol{\rho}_j\boldsymbol{\rho}_j^T\right)
\end{aligned} \tag{A.7}$$

$$\mathbf{H}_{\widehat{\boldsymbol{\phi}}_{ni}} = -2\widehat{\boldsymbol{\Delta}}_{ni} + 2\overline{\alpha}_{ni}\mathbf{I}_{N_i} \tag{A.8}$$

where $\mathbf{I}_{N_i} = \sum_{j=1}^{N_i} \boldsymbol{\rho}_j\boldsymbol{\rho}_j^T$, $\boldsymbol{\rho}_1 = \widehat{\boldsymbol{\phi}}_{ni}$, $\widehat{\boldsymbol{\phi}}_{ni}^T\widehat{\boldsymbol{\phi}}_{ni} = 1$, $\widehat{\boldsymbol{\phi}}_{ni}^T\boldsymbol{\rho}_j = 0$, $\widehat{\boldsymbol{\phi}}_{ni}^T\widehat{\boldsymbol{\Delta}}_{ni}\widehat{\boldsymbol{\phi}}_{ni} = \widehat{\boldsymbol{\phi}}_{ni}^T\overline{\alpha}_{ni}\widehat{\boldsymbol{\phi}}_{ni} = \widehat{\alpha}_{ni}$, and. $\widehat{\boldsymbol{\phi}}_{ni}^T\mathbf{H}_{\widehat{\boldsymbol{\phi}}_i}\widehat{\boldsymbol{\phi}}_{ni} = 0$.

Derivative of $\boldsymbol{\Delta}_{ni}$ with respect to $\boldsymbol{\Theta}_{s,ni}$ can be obtained as follows.

$$\frac{\partial \boldsymbol{\Delta}_{ni}}{\partial \boldsymbol{\Theta}_{s,ni}} = \sum_k \frac{\partial}{\partial \boldsymbol{\Theta}_{s,ni}}\left[\frac{\overline{S}_{ni}D_{kni}}{S_{e,ni}(\overline{S}_{ni}D_{k,ni} + S_{e,ni})}\right] \mathrm{Re}(\mathbf{F}_{ki}\mathbf{F}_{ki}^*) \tag{A.9}$$

In Eq. (A.9), it is seen that the derivative of $\boldsymbol{\Delta}_{ni}$ is a Hermitian matrix. Therefore, its eigenvalue decomposition should also be Hermitian.

$$\begin{aligned}
\boldsymbol{\Delta}_{ni} &= \sum_{i=1}^{N} \sigma_i\boldsymbol{\rho}_i\boldsymbol{\rho}_i^T \\
\frac{\partial \boldsymbol{\Delta}_{ni}}{\partial \boldsymbol{\Theta}_{s,ni}} &= \sum_{i=1}^{N} \frac{\partial \sigma_i}{\partial \boldsymbol{\Theta}_{s,ni}}\boldsymbol{\rho}_i\boldsymbol{\rho}_i^T + \sigma_i\frac{\partial \boldsymbol{\rho}_i}{\partial \boldsymbol{\Theta}_{s,ni}}\boldsymbol{\rho}_i^T + \sigma_i\rho_i\frac{\partial \boldsymbol{\rho}_i^T}{\partial \boldsymbol{\Theta}_{s,ni}}
\end{aligned} \tag{A.10}$$

where $\partial\boldsymbol{\rho}_i/\partial\boldsymbol{\Theta}_{s,ni}$ will be orthogonal to $\boldsymbol{\rho}_i$. Therefore, $\partial\boldsymbol{\rho}_i/\partial\boldsymbol{\Theta}_{s,ni}$ should be equal to zero in order to keep Hermitian structure of $\partial\boldsymbol{\Delta}_{ni}/\partial\boldsymbol{\Theta}_{s,ni}$. Thus, the derivative of $\boldsymbol{\Delta}(\boldsymbol{\Theta}_{s,ni})$ is obtained as below.

$$\frac{\partial \boldsymbol{\Delta}_{ni}}{\partial \boldsymbol{\Theta}_{s,ni}} = \sum_{i=1}^{N} \frac{\partial \sigma_i}{\partial \boldsymbol{\Theta}_{s,ni}}\boldsymbol{\rho}_i\boldsymbol{\rho}_i^T = \frac{\partial \overline{\alpha}_{ni}}{\partial \boldsymbol{\Theta}_{s,ni}}\boldsymbol{\phi}_{ni}\boldsymbol{\phi}_{ni}^T + \sum_{i=2}^{N} \frac{\partial \sigma_i}{\partial \boldsymbol{\Theta}_{s,ni}}\boldsymbol{\rho}_i\boldsymbol{\rho}_i^T \tag{A.11}$$

Thus, a zero correlation is obtained between $\boldsymbol{\Theta}_{s,ni}$ and $\boldsymbol{\phi}_{ni}$ by making use of Eqs. (A.7) and (A.11), as follows.

$$\begin{aligned}
\mathbf{H}_{\widehat{\boldsymbol{\Theta}}_{sni}\widehat{\boldsymbol{\phi}}_{ni}} &= \widehat{\boldsymbol{\phi}}_{ni}^T \times \frac{\partial \boldsymbol{\Delta}_{ni}}{\partial \boldsymbol{\Theta}_{sni}}\bigg|_{\boldsymbol{\Theta}_{sni}=\widehat{\boldsymbol{\Theta}}_{sni}} \times \left(0 \times \widehat{\boldsymbol{\phi}}_{ni}\widehat{\boldsymbol{\phi}}_{ni}^T - \sum_{j=2}^{N_i} \boldsymbol{\rho}_j\boldsymbol{\rho}_j^T\right) \\
&= \frac{\partial \widehat{\overline{\alpha}}_{ni}}{\partial \boldsymbol{\Theta}_{sni}}\widehat{\boldsymbol{\phi}}_{ni}^T \times \left(0 \times \widehat{\boldsymbol{\phi}}_{ni}\widehat{\boldsymbol{\phi}}_{ni}^T - \sum_{j=2}^{N_i} \boldsymbol{\rho}_j\boldsymbol{\rho}_j^T\right) = 0
\end{aligned} \tag{A.12}$$

Appendix B

Derivatives of the objective function

- Derivative of $J^{(\theta,\theta)}$

$$J^{(\theta,\theta)} = \left.\frac{\partial^2 J}{\partial \theta^2}\right|_{\theta=\widehat{\theta},\rho=\widehat{\rho},\chi=\widehat{\chi}} = S_{\theta_{ro}}^{-1}\mathbf{I}_{N\times N} + \sum_{n=1}^{N_m} S_{\varepsilon_n}^{-1}\mathbf{G}_{K_n}^{T}\mathbf{G}_{K_n} \tag{B.1}$$

- Derivative of $J^{(\theta,\rho)}$

$$J^{(\theta,\rho)} = \{J^{(\rho,\theta)}\}^{T} = \left.\frac{\partial^2 J}{\partial \boldsymbol{\theta}\partial \boldsymbol{\rho}}\right|_{\theta=\widehat{\theta},\rho=\widehat{\rho},\chi=\widehat{\chi}} = -\sum_{n=1}^{N_m} S_{\varepsilon_n}^{-1}\mathbf{G}_{K_n}^{T}\mathbf{G}_{M_n} \tag{B.2}$$

- Derivative of $J^{(\theta,\lambda)}$

$$\begin{aligned} J^{(\theta,\lambda)} = \{J^{(\lambda,\theta)}\}^{T} &= \left.\frac{\partial^2 J}{\partial \theta\partial \lambda}\right|_{\theta=\widehat{\theta},\rho=\widehat{\rho},\chi=\widehat{\chi}} = \left[\, J^{(\theta,\lambda_1)} \quad \dots \quad J^{(\theta,\lambda_{N_m})} \,\right]_{N_\theta\times N_m} \\ J^{(\theta,\lambda_1)} &= -S_{\widehat{\varepsilon}}^{-1}\mathbf{G}_{K_n}^{T}\mathbf{M}(\boldsymbol{\rho})\boldsymbol{\Phi}_n \end{aligned} \tag{B.3}$$

- Derivative of $J^{(\theta,\Phi)}$

$$\begin{aligned} J^{(\theta,\Phi)} = \{J^{(\Phi,\theta)}\}^{T} &= \left.\frac{\partial^2 J}{\partial \boldsymbol{\theta}\partial \boldsymbol{\Phi}}\right|_{\theta=\widehat{\theta},\rho=\widehat{\rho},\chi=\widehat{\chi}} = \left[\, J^{(\theta,\Phi_1)} \quad \dots \quad J^{(\theta,\Phi_{N_m})} \,\right]_{N_\theta\times N_m N} \\ J^{(\theta,\Phi_n)} &= \left[\, \{J^{(\theta_1,\Phi_n)}\}^{T} \quad \dots \quad \{J^{(\theta_{N_\theta},\Phi_n)}\}^{T} \,\right]_{N\times N_\theta}^{T} \\ J^{(\theta_i,\Phi_n)} &= \left[2S_{\widehat{\varepsilon}}^{-1}\widehat{\boldsymbol{\Phi}}_n^{T}\boldsymbol{\Omega}_n\mathbf{K}_i\left(\mathbf{I}_N - \widehat{\boldsymbol{\Phi}}_n\widehat{\boldsymbol{\Phi}}_n^{T}\right)\right]_{1\times N} \end{aligned} \tag{B.4}$$

- Derivative of $J^{(\rho,\rho)}$

$$J^{(\rho,\rho)} = \left.\frac{\partial^2 J}{\partial \boldsymbol{\rho}^2}\right|_{\theta=\widehat{\theta},\rho=\widehat{\rho},\chi=\widehat{\chi}} = S_{\widehat{\rho}_o}^{-1}\mathbf{I}_{N\times N} + \sum_{n=1}^{N_m} S_{\widehat{\varepsilon}}^{-1}\mathbf{G}_{M_n}^{T}\mathbf{G}_{M_n} \tag{B.5}$$

- Derivative of $J^{(\rho,\lambda)}$

$$\begin{aligned} \mathbf{J}^{(\boldsymbol{\rho},\boldsymbol{\lambda})} &= \{\mathbf{J}^{(\boldsymbol{\lambda},\boldsymbol{\rho})}\}^{\mathrm{T}} = \left.\frac{\partial^2 J}{\partial \boldsymbol{\rho}\partial\boldsymbol{\lambda}}\right|_{\boldsymbol{\theta}=\widehat{\boldsymbol{\theta}},\boldsymbol{\rho}=\widehat{\boldsymbol{\rho}},\boldsymbol{\chi}=\widehat{\boldsymbol{\chi}}} = \left[\mathbf{J}^{(\boldsymbol{\rho},\lambda_1)} \quad \ldots \quad \mathbf{J}^{(\boldsymbol{\rho},\lambda_{N_m})}\right]_{N_\rho \times N_m} \\ \mathbf{J}^{(\boldsymbol{\rho},\lambda_n)} &= \mathbf{S}_{\widehat{\varepsilon}}^{-1}\left(2\lambda_n \tilde{\mathbf{G}}_{M_n}^{\mathrm{T}}\mathbf{G}_{M_n}\widehat{\boldsymbol{\rho}} - \tilde{\mathbf{G}}_{M_n}^{\mathrm{T}}\mathbf{g}_{M_n} + \mathbf{G}_{M_n}^{\mathrm{T}}\mathbf{M}_0\widehat{\boldsymbol{\Phi}}_n\right) \end{aligned} \tag{B.6}$$

where

$$\tilde{\mathbf{G}}_{M_n} = \left[\mathbf{M}_1\widehat{\boldsymbol{\Phi}}_n \quad \ldots \quad \mathbf{M}_{N_{el}}\widehat{\boldsymbol{\Phi}}_n\right]_{N\times N_\rho} \tag{B.7}$$

- Derivative of $\mathbf{J}^{(\boldsymbol{\rho},\boldsymbol{\Phi})}$

$$\begin{aligned} \mathbf{J}^{(\boldsymbol{\rho},\boldsymbol{\Phi})} &= \{\mathbf{J}^{(\boldsymbol{\Phi},\boldsymbol{\rho})}\}^{\mathrm{T}} = \left.\frac{\partial^2 J}{\partial\boldsymbol{\theta}\partial\boldsymbol{\lambda}}\right|_{\boldsymbol{\theta}=\widehat{\boldsymbol{\theta}},\boldsymbol{\rho}=\widehat{\boldsymbol{\rho}},\boldsymbol{\chi}=\widehat{\boldsymbol{\chi}}} = \left[\mathbf{J}^{(\boldsymbol{\rho},\boldsymbol{\Phi}_1)} \quad \ldots \quad \mathbf{J}^{(\boldsymbol{\rho},\boldsymbol{\Phi}_{N_m})}\right]_{N_\rho\times N_m N} \\ \mathbf{J}^{(\boldsymbol{\rho},\boldsymbol{\Phi}_n)} &= \left[\{\mathbf{J}^{(\boldsymbol{\rho}_1,\boldsymbol{\Phi}_n)}\}^{\mathrm{T}} \quad \ldots \quad \{\mathbf{J}^{(\boldsymbol{\rho}_{N_\theta},\boldsymbol{\Phi}_n)}\}^{\mathrm{T}}\right]^{\mathrm{T}}_{N\times N_\rho} \\ \mathbf{J}^{(\rho_m,\boldsymbol{\Phi}_n)} &= \left[2S_{\widehat{\varepsilon}}^{-1}\widehat{\boldsymbol{\Phi}}_n^{\mathrm{T}}\boldsymbol{\Omega}_n\lambda_n\mathbf{M}_i\left(\mathbf{I}_N - \widehat{\boldsymbol{\Phi}}_n\widehat{\boldsymbol{\Phi}}_n^{\mathrm{T}}\right)\right]_{1\times N} \end{aligned} \tag{B.8}$$

- Derivative of $\mathbf{J}^{(\boldsymbol{\lambda},\boldsymbol{\lambda})}$

$$\mathbf{J}^{(\boldsymbol{\lambda},\boldsymbol{\lambda})} = \left.\frac{\partial^2 J}{\partial\boldsymbol{\lambda}^2}\right|_{\boldsymbol{\theta}=\widehat{\boldsymbol{\theta}},\boldsymbol{\rho}=\widehat{\boldsymbol{\rho}},\boldsymbol{\chi}=\widehat{\boldsymbol{\chi}}} = \left[\mathrm{diag}\left(S_{\widehat{\varepsilon}}^{-1}G_{\widehat{\lambda}_n} + \sum_{i=1}^{N_s} H_{\widehat{\lambda}_{ni}}\right)\right]_{N_m\times N_m} \tag{B.9}$$

- Derivative of $\mathbf{J}^{(\boldsymbol{\lambda},\boldsymbol{\Phi})}$

$$\begin{aligned} \mathbf{J}^{(\boldsymbol{\lambda},\boldsymbol{\Phi})} &= \{\mathbf{J}^{(\boldsymbol{\Phi},\boldsymbol{\lambda})}\}^{\mathrm{T}} = \left.\frac{\partial^2 J}{\partial\boldsymbol{\Phi}\partial\boldsymbol{\lambda}}\right|_{\boldsymbol{\theta}=\widehat{\boldsymbol{\theta}},\boldsymbol{\rho}=\widehat{\boldsymbol{\rho}},\boldsymbol{\chi}=\widehat{\boldsymbol{\chi}}} = \left[\mathbf{J}^{(\boldsymbol{\lambda},\boldsymbol{\Phi}_1)} \quad \ldots \quad \mathbf{J}^{(\boldsymbol{\lambda},\boldsymbol{\Phi}_{N_m})}\right]_{N\times N_m N} \\ \mathbf{J}^{(\boldsymbol{\lambda},\boldsymbol{\Phi}_n)} &= \left[\{\mathbf{J}^{(\lambda_1,\boldsymbol{\Phi}_n)}\}^{\mathrm{T}} \quad \ldots \quad \{\mathbf{J}^{(\lambda_{N_m},\boldsymbol{\Phi}_n)}\}^{\mathrm{T}}\right]^{\mathrm{T}}_{N_m N\times N} \\ \mathbf{J}^{(\lambda_m,\Phi_n)} &= \begin{cases} \left[-2\widehat{S}_{\widehat{\varepsilon}}^{-1}\widehat{\boldsymbol{\Phi}}_n^{\mathrm{T}}\boldsymbol{\Omega}_n\mathbf{M}(\boldsymbol{\rho})\left(\mathrm{I}_N - \widehat{\boldsymbol{\Phi}}_n\widehat{\boldsymbol{\Phi}}_n^{\mathrm{T}}\right)\right]_{1\times N} & \text{if } n = m \\ \mathbf{0}_{1\times N} & \text{otherwise} \end{cases} \end{aligned} \tag{B.10}$$

- Derivative of $J^{(\boldsymbol{\Phi},\boldsymbol{\Phi})}$

$$J^{(\boldsymbol{\Phi},\boldsymbol{\Phi})} = \left.\frac{\partial^2 J}{\partial \boldsymbol{\Phi}^2}\right|_{\boldsymbol{\theta}=\widehat{\boldsymbol{\theta}},\rho=\widehat{\rho},\chi=\widehat{\chi}} = \mathrm{diag}[\, J^{(\boldsymbol{\Phi}_1,\boldsymbol{\Phi}_1)} \quad \ldots \quad J^{(\boldsymbol{\Phi}_{N_m},\boldsymbol{\Phi}_{N_m})}\,]_{N_m N \times N_m N}$$
$$J^{(\boldsymbol{\Phi}_n,\boldsymbol{\Phi}_n)} = \left\{ \sum_{i=1}^{N_s} \boldsymbol{\Gamma}_{oi}^T \left(r_{ni}^{-2} \mathbf{H}_{\widehat{\phi}_i} + 2\alpha_{ni} I_{N_i} \right) \boldsymbol{\Gamma}_{oi} \right\} + \boldsymbol{\Omega}_n^T S_{\widehat{\varepsilon}}^{-1} \boldsymbol{\Omega}_n - 2\beta_n \mathbf{I}_N \tag{B.11}$$

Appendix C

Non-parametric substructure stiffness and mass matrices for the presented numerical example

- Stiffness matrix, K_r;

For r = 1,

$$\mathbf{K}_{1x} = k_{1x} \begin{bmatrix} \begin{bmatrix} 1 & 0 & 0 & -1 & 0 & 0 \\ 0 & 0 & 0 & 0 & 0 & 0 \\ 0 & 0 & L_x^2/4 & 0 & 0 & 0 \\ 0 & 0 & 0 & 0 & 0 & 0 \\ 0 & 0 & 0 & 0 & 0 & 0 \\ 0 & 0 & 0 & 0 & 0 & 0 \end{bmatrix} & \mathbf{0}_{6\times 39} \\ \mathbf{0}_{39\times 45} \end{bmatrix} \tag{C.1}$$

$$\mathbf{K}_{1y} = k_{1y} \begin{bmatrix} \begin{bmatrix} 0 & 0 & 0 & 0 & 0 & 0 \\ 0 & 1 & 0 & 0 & -1 & 0 \\ 0 & 0 & L_y^2/4 & 0 & 0 & 0 \\ 0 & 0 & 0 & 0 & 0 & 0 \\ 0 & 0 & 0 & 0 & 0 & 0 \\ 0 & 0 & 0 & 0 & 0 & 0 \end{bmatrix} & \mathbf{0}_{6\times 39} \\ \mathbf{0}_{39\times 45} \end{bmatrix} \tag{C.2}$$

For r = 2, 3, 4,…, 15

$$\mathbf{K}_{rx} = k_{rx}\begin{bmatrix} \mathbf{0}_{3(r-2)\times 45} \\ \mathbf{0}_{1\times 3(r-2)} \begin{bmatrix} 1 & 0 & 0 & -1 & 0 & 0 \\ 0 & 0 & 0 & 0 & 0 & 0 \\ 0 & 0 & L_x^2/4 & 0 & 0 & -L_x^2/4 \\ -1 & 0 & 0 & 1 & 0 & 0 \\ 0 & 0 & 0 & 0 & 0 & 0 \\ 0 & 0 & -L_x^2/4 & 0 & 0 & L_x^2/4 \end{bmatrix} \mathbf{0}_{1\times 3(15-r)} \\ \mathbf{0}_{3(15-r)\times 45} \end{bmatrix} \tag{C.3}$$

$$\mathbf{K}_{ry} = k_{ry}\begin{bmatrix} \mathbf{0}_{3(r-2)\times 45} \\ \mathbf{0}_{1\times 3(r-2)} \begin{bmatrix} 0 & 0 & 0 & 0 & 0 & 0 \\ 0 & 1 & 0 & 0 & -1 & 0 \\ 0 & 0 & L_y^2/4 & 0 & 0 & -L_y^2/4 \\ 0 & 0 & 0 & 0 & 0 & 0 \\ 0 & -1 & 0 & 0 & 1 & 0 \\ 0 & 0 & -L_y^2/4 & 0 & 0 & L_y^2/4 \end{bmatrix} \mathbf{0}_{1\times 3(15-r)} \\ \mathbf{0}_{3(15-r)\times 45} \end{bmatrix} \tag{C.4}$$

where, $k_{rx} = k_{rx\text{-}} + k_{rx+}$ and $k_{ry} = k_{ry\text{-}} + k_{ry+}$.

- Mass matrix, $\mathbf{M}_r$;

  For $r = 1$,

$$\mathbf{M}_1 = \mathrm{m}\begin{bmatrix} \begin{bmatrix} 1 & 0 & 0 & 0 & 0 & 0 \\ 0 & 1 & 0 & 0 & 0 & 0 \\ 0 & 0 & \frac{\left(L_x^2+L_y^2\right)}{12} & 0 & 0 & 0 \\ 0 & 0 & 0 & 0 & 0 & 0 \\ 0 & 0 & 0 & 0 & 0 & 0 \\ 0 & 0 & 0 & 0 & 0 & 0 \end{bmatrix} & \mathbf{0}_{6\times 39} \\ \mathbf{0}_{39\times 45} \end{bmatrix} \tag{C.5}$$

For r = 2,…, 14

$$\mathbf{M}_r = \mathrm{m}\begin{bmatrix} \mathbf{0}_{3(r-2)\times 45} \\ \begin{bmatrix} \mathbf{0}_{1\times 3(r-2)} & \begin{bmatrix} 1/2 & 0 & 0 & 0 & 0 & 0 \\ 0 & 1/2 & 0 & 0 & 0 & 0 \\ 0 & 0 & \frac{\left(L_x^2+L_y^2\right)}{24} & 0 & 0 & 0 \\ 0 & 0 & 0 & 1/2 & 0 & 0 \\ 0 & 0 & 0 & 0 & 1/2 & 0 \\ 0 & 0 & 0 & 0 & 0 & \frac{\left(L_x^2+L_y^2\right)}{24} \end{bmatrix} & \mathbf{0}_{1\times 3(15-r)} \end{bmatrix} \\ \mathbf{0}_{3(15-r)\times 45} \end{bmatrix} \tag{C.6}$$

For r = 15

$$\mathbf{M}_{15} = \mathrm{m}\begin{bmatrix} \mathbf{0}_{39\times 45} \\ \begin{bmatrix} \mathbf{0}_{6\times 39} & \begin{bmatrix} 1/2 & 0 & 0 & 0 & 0 & 0 \\ 0 & 1/2 & 0 & 0 & 0 & 0 \\ 0 & 0 & \frac{\left(L_x^2+L_y^2\right)}{24} & 0 & 0 & 0 \\ 0 & 0 & 0 & 1 & 0 & 0 \\ 0 & 0 & 0 & 0 & 1 & 0 \\ 0 & 0 & 0 & 0 & 0 & \frac{\left(L_x^2+L_y^2\right)}{12} \end{bmatrix} \end{bmatrix} \end{bmatrix} \tag{C.7}$$

References

[1] K. Yuen, Bayesian Methods for Structural Dynamics and Civil Engineering, John Wiley & Sons (Asia) Pte Ltd, 2010.
[2] B.N. Datta, Finite-element model updating, eigenstructure assignment and eigenvalue embedding techniques for vibrating systems, Mech. Syst. Signal Process. 16 (2002) 83–96, https://doi.org/10.1006/mssp.2001.1443.
[3] J.R. Fonseca, M.I. Friswell, J.E. Mottershead, A.W. Lees, Uncertainty identification by the maximum likelihood method, J. Sound Vib. 288 (2005) 587–599, https://doi.org/10.1016/j.jsv.2005.07.006.
[4] T. Ma, Y. Zhang, X. Huang, A novel approach for stochastic finite element model updating and parameter estimation, Proc. Inst. Mech. Eng. C J. Mech. Eng. Sci. 228 (2014) 3329–3342, https://doi.org/10.1177/0954406214529945.
[5] J.E. Mottershead, M.I. Friswel, Model updating in structural dynamics: a survey, J. Sound Vib. 167 (1993) 347–375.
[6] J.E. Mottershead, M. Link, M.I. Friswell, The sensitivity method in finite element model updating: a tutorial, Mech. Syst. Signal Process. 25 (2011) 2275–2296, https://doi.org/10.1016/j.ymssp.2010.10.012.
[7] N. Touat, N. Benseddiq, A. Ghoul, S. Rechak, An accelerated pseudo-genetic algorithm for dynamic finite element model updating, Eng. Optim. 46 (2014) 340–360, https://doi.org/10.1080/0305215X.2013.772600.
[8] M.K. Vakilzadeh, V. Yaghoubi, A.T. Johansson, T.J.S. Abrahamsson, Stochastic finite element model calibration based on frequency responses and bootstrap sampling, Mech. Syst. Signal Process. 88 (2017) 180–198, https://doi.org/10.1016/j.ymssp.2016.11.014.
[9] S.E. Fang, Q.H. Zhang, W.X. Ren, Parameter variability estimation using stochastic response surface model updating, Mech. Syst. Signal Process. 49 (2014) 249–263, https://doi.org/10.1016/j.ymssp.2014.04.017.
[10] C. Mares, J.E. Mottershead, M.I. Friswell, Stochastic model updating: Part 1-theory and simulated example, Mech. Syst. Signal Process. 20 (2006) 1674–1695, https://doi.org/10.1016/j.ymssp.2005.06.006.
[11] J.E. Mottershead, C. Mares, S. James, M.I. Friswell, Stochastic model updating: Part 2-application to a set of physical structures, Mech. Syst. Signal Process. 20 (2006) 2171–2185, https://doi.org/10.1016/j.ymssp.2005.06.007.
[12] S.E. Fang, W.X. Ren, R. Perera, A stochastic model updating method for parameter variability quantification based on response surface models and Monte Carlo simulation, Mech. Syst. Signal Process. 33 (2012) 83–96, https://doi.org/10.1016/j.ymssp.2012.06.028.
[13] M.I. Friswell, The adjustment of structural parameters using a minimum variance estimator, Mech. Syst. Signal Process. 3 (1989) 143–155, https://doi.org/10.1016/0888-3270(89)90013-7.
[14] H.H. Khodaparast, J.E. Mottershead, M.I. Friswell, Perturbation methods for the estimation of parameter variability in stochastic model updating, Mech. Syst. Signal Process. 22 (2008) 1751–1773, https://doi.org/10.1016/j.ymssp.2008.03.001.
[15] N. Abu Husain, H. Haddad Khodaparast, H. Ouyang, Parameter selection and stochastic model updating using perturbation methods with parameter weighting matrix assignment, Mech. Syst. Signal Process. 32 (2012) 135–152, https://doi.org/10.1016/j.ymssp.2012.04.001.
[16] C. Soize, E. Capiez-Lernout, R. Ohayon, Robust updating of uncertain computational models using experimental modal analysis, AIAA J. 46 (2008) 2955–2965, https://doi.org/10.2514/1.38115.
[17] S. Bansal, A new gibbs sampling based bayesian model updating approach using modal data from multiple setups, Int. J. Uncertain. Quantification 5 (2015) 361–374, https://doi.org/10.1615/int.j.uncertaintyquantification.2015013581.
[18] J. Jang, A. Smyth, Bayesian model updating of a full-scale finite element model with sensitivity-based clustering, Struct. Control Health Monit. 24 (2017) 1–15, https://doi.org/10.1002/stc.2004.
[19] S. Mustafa, N. Debnath, A. Dutta, Bayesian probabilistic approach for model updating and damage detection for a large truss bridge, Int. J. Steel Struct. 15 (2015) 473–485, https://doi.org/10.1007/s13296-015-6016-3.
[20] S. Mustafa, Y. Matsumoto, Bayesian model updating and its limitations for detecting local damage of an existing truss bridge, J. Bridge Eng. 22 (2017), https://doi.org/10.1061/(asce)be.1943-5592.0001044, 04017019.
[21] E. Patelli, Y. Govers, M. Broggi, H.M. Gomes, M. Link, J.E. Mottershead, Sensitivity or Bayesian model updating: a comparison of techniques using the DLR AIRMOD test data, Arch. Appl. Mech. 87 (2017) 905–925, https://doi.org/10.1007/s00419-017-1233-1.
[22] K. Prajapat, S. Ray-Chaudhuri, Detection of multiple damages employing best achievable eigenvectors under Bayesian inference, J. Sound Vib. 422 (2018) 237–263, https://doi.org/10.1016/j.jsv.2018.02.012.
[23] J.L. Beck, L.S. Katafygiostis, Updating models and their uncertainties I: Bayesian statistical frameworks, J. Eng. Mech. 124 (1998) 455–461.
[24] J.L. Beck, S.-K. Au, Bayesian updating of structural models and reliability using Markov chain Monte Carlo simulation, J. Eng. Mech. 128 (2002) 380–391, https://doi.org/10.1061/(asce)0733-9399, 2002)128:4(380).
[25] I. Behmanesh, B. Moaveni, G. Lombaert, C. Papadimitriou, Hierarchical Bayesian model updating for structural identification, Mech. Syst. Signal Process. 64–65 (2015) 360–376, https://doi.org/10.1016/j.ymssp.2015.03.026.
[26] J. Ching, Y. Chen, Transitional Markov chain Monte Carlo method for bayesian model updating, model class selection, and model averaging, J. Eng. Mech. 133 (2007) 816–832, https://doi.org/10.1061/(ASCE)0733-9399, 2007)133:7(816) CE.
[27] I. Boulkaibet, L. Mthembu, T. Marwala, M.I. Friswell, S. Adhikari, Finite element model updating using an evolutionary Markov chain Monte Carlo algorithm, in: J. Caicedo, S. Pakzad (Eds.), Dyn. Civ. Struct., Conference Proceedings of the Society for Experimental Mechanics Series., 2, Springer, Cham, 2015, pp. 245–253.
[28] S.H. Cheung, S. Bansal, A new Gibbs sampling based algorithm for Bayesian model updating with incomplete complex modal data, Mech. Syst. Signal Process. 92 (2017) 156–172, https://doi.org/10.1016/j.ymssp.2017.01.015.
[29] N. Metropolis, A.W. Rosenbluth, M.N. Rosenbluth, A.H. Teller, Equation of state calculations by fast computing machine, J. Chem. Phys. 21 (1953) 1087–1092, https://doi.org/10.1063/1.1699114.
[30] J. Ching, J.L. Beck, New Bayesian model updating algorithm applied to a structural health monitoring benchmark, Struct. Health Monit. 3 (2004) 313–332, https://doi.org/10.1177/1475921704047499.
[31] K. Yuen, L.S. Katafygiotis, Bayesian fast fourier Transform approach for modal updating using ambient data, Adv. Struct. Eng. 6 (2003) 81–95, https://doi.org/10.1260/136943303769013183.
[32] K.V. Yuen, L.S. Katafygiotis, Bayesian time-domain approach for modal updating using ambient data, Probabilistic Eng. Mech. 16 (2001) 219–231, https://doi.org/10.1016/S0266-8920(01)00004-2.
[33] L.S. Katafygiotis, K.V. Yuen, Bayesian spectral density approach for modal updating using ambient data, Earthq. Eng. Struct. Dyn. 30 (2001) 1103–1123, https://doi.org/10.1002/eqe.53.
[34] K.-V. Yuen, S.-C. Kuok, Bayesian methods for updating dynamic models, Appl. Mech. Rev. 64 (2011), 010802, https://doi.org/10.1115/1.4004479.
[35] W.J. Yan, L.S. Katafygiotis, A novel Bayesian approach for structural model updating utilizing statistical modal information from multiple setups, Struct. Saf. 52 (2015) 260–271, https://doi.org/10.1016/j.strusafe.2014.06.004.
[36] S. Au, F. Zhang, Fundamental two-stage formulation for Bayesian system identification , Part I : general theory, Mech. Syst. Signal Process. 66–67 (2016) 31–42, https://doi.org/10.1016/j.ymssp.2015.04.025.
[37] F.L. Zhang, S.K. Au, Fundamental two-stage formulation for Bayesian system identification, Part II: application to ambient vibration data, Mech. Syst. Signal Process. 66–67 (2016) 43–61, https://doi.org/10.1016/j.ymssp.2015.04.024.
[38] F.L. Zhang, Y.C. Ni, H.F. Lam, Bayesian structural model updating using ambient vibration data collected by multiple setups, Struct. Control Health Monit. 24 (2017) 1–18, https://doi.org/10.1002/stc.2023.
[39] S.-K. Au, Fast bayesian FFT method for ambient modal identification with separated modes, J. Eng. Mech. 137 (2011) 214–226, https://doi.org/10.1061/(asce)em.1943-7889.0000213.
[40] S.K. Au, Y.L. Xie, Calculation of Hessian under constraints with applications to Bayesian system identification, Comput. Methods Appl. Mech. Eng. 323 (2017) 373–388, https://doi.org/10.1016/j.cma.2017.05.021.

[41] Ç. Hızal, G. Turan, E. Aktaş, H. Ceylan, A mode shape assembly algorithm by using two stage Bayesian Fast Fourier Transform Approach, Mech. Syst. Signal Process. 134 (2019) 106328, https://doi.org/10.1016/j.ymssp.2019.106328.
[42] S.K. Au, F.L. Zhang, On assessing the posterior mode shape uncertainty in ambient modal identification, Probabilistic Eng. Mech. 26 (2011) 427–434, https://doi.org/10.1016/j.probengmech.2010.11.009.
[43] M.W. Vanik, J.L. Beck, S.K. Au, Bayesian probabilistic approach to structural health monitoring, J. Eng. Mech. 126 (2002) 738–745, https://doi.org/10.1061/(asce)0733-9399, 2000)126:7(738).
[44] E.L. Zhang, P. Feissel, J. Antoni, A comprehensive Bayesian approach for model updating and quantification of modeling errors, Probabilistic Eng. Mech. 26 (2011) 550–560, https://doi.org/10.1016/j.probengmech.2011.07.001.
[45] F.L. Zhang, S.K. Au, Probabilistic model for modal properties based on operational modal analysis, ASCE-ASME J. Risk Uncertain. Eng. Syst. Part A Civ. Eng. 2 (2016), https://doi.org/10.1061/ajrua6.0000843. B4015005.